

RESEARCH ARTICLE

10.1029/2017JB014861

Key Points:

- Mesozoic volcanic arc in the present-day SCS continental margin is inferred
- The opening of the SCS basins has broken the arc area in the southwest and the forearc area in the northeast margin; the Reed Bank is connected with the Zhongsha and Xisha Islands before breakup

Correspondence to:

Z. Sun and H. Yang,
zhensun@scsio.ac.cn;
hyang@cuhk.edu.hk

Citation:

Li, F., Sun, Z., & Yang, H. (2018). Possible spatial distribution of the Mesozoic volcanic arc in the present-day South China Sea continental margin and its tectonic implications. *Journal of Geophysical Research: Solid Earth*, 123, 6215–6235. <https://doi.org/10.1029/2017JB014861>

Received 14 AUG 2017

Accepted 17 JUL 2018

Accepted article online 26 JUL 2018

Published online 22 AUG 2018

Possible Spatial Distribution of the Mesozoic Volcanic Arc in the Present-Day South China Sea Continental Margin and Its Tectonic Implications

Fucheng Li^{1,2}, Zhen Sun¹ , and Hongfeng Yang³ 

¹CAS Key Laboratory of Ocean and Marginal Sea Geology, South China Sea Institute of Oceanology, Chinese Academy of Sciences, Guangzhou, China, ²Key Laboratory of Marine Geology and Environment, Institute of Oceanology, Chinese Academy of Sciences, Qingdao, China, ³Earth System Science Programme, Faculty of Science, The Chinese University of Hong Kong, Hong Kong

Abstract The distribution of the Late Mesozoic volcanic arc in the South China Sea (SCS) continental margin has long been a controversial topic due to its significance in understanding the transition mechanism of a margin from subduction to extension. Here a comprehensive analysis was conducted in the margin using reprocessed magnetic data, newly collected drilling/dredging samples, depositional environment, and deformation style inferred from multichannel seismic profiles to jointly constrain the possible distribution of the Mesozoic volcanic arc. From the map of reduced-to-the-pole magnetic anomaly, several high-positive magnetic anomaly belts can be discriminated, which cross the central Pearl River Mouth Basin, extend southwestward to the Zhongsha (Macclesfield Bank) and Xisha Islands (Paracel Islands), and distribute discontinuously around the southwest subbasin. Geophysical analysis shows that these belts have similar amplitudes and magnetic depths to known volcanic arcs, such as the Luzon, Cagayan, and Sulu arcs. Furthermore, the high-amplitude positive magnetic anomaly belts coincide with the distribution of Late Mesozoic arc-like granites, intermediate rocks, and agglomerates, suggesting that the belts possibly originated from the existence of Late Mesozoic volcanic arc. Accretion and compression environment located in front of the inferred arc provides independent supports to our interpretation. Results indicate that the southwest part of the arc is distributed on both sides of the southwest SCS subbasin, whereas the northeast part remains nearly in its original location, further suggesting that the breakup locations for the SCS margin might be the volcanic front/forearc in the northeast and the arc in the southwest during the opening of the SCS basin.

1. Introduction

The South China Sea (SCS), which is bounded by the Eurasian, India, Australian, and the Philippine Sea plates, is one of the largest marginal seas in the southeast margin of the Eurasian continent (Figure 1). Aside from the oceanic basin, the SCS consists of two submarine continental margins, namely, the northern and southern continental margins. Numerous studies have been conducted to investigate the Cenozoic tectonic evolution of the SCS. These studies have reached a consensus that the SCS margin was passive and evolved from continental rifting to seafloor spreading since the Early Cenozoic, resulting in several extensional basins, such as the Pearl River Mouth Basin (PRMB), the Tainan Basin, and the Qiongdongnan Basin (e.g., S. Chen et al., 1987; Gong et al., 1997; S. Li, Lin, et al., 1999; Ru & Pigott, 1986; J. Wu, 1994).

In comparison with the extensive investigations on the Cenozoic tectonic evolution of the SCS margins, the Mesozoic tectonic setting is considerably less understood. Widespread onshore outcrops of the Late Mesozoic granitic-volcanic rocks show that the SCS was once an active margin associated with Paleo-Pacific subduction in the Late Mesozoic Yanshanian Period (180–66 Ma; J. Chen & Jahn, 1998; Gilder et al., 1996; S. Sun et al., 1989; Zamoras & Matsuoka, 2001; X. Zhou & Li, 2000). The corresponding onshore magmatic arc extends from the South China coastal line to the Indochina Peninsula, and several Late Cretaceous back-arc sedimentary basins have developed landward of the arc (X. M. Zhou, Sun, et al., 2006; Figure 1).

In the northern SCS margin, a similar Mesozoic magmatic arc has been suggested and viewed as a submarine elongation of the onshore arc based on geochemical and geophysical analyses (Figure 1; e.g., Xia & Huang, 2004; Yao et al., 1994; D. Zhou, Wang, et al., 2006). For example, the compositional characteristic analysis of several drilling samples shows that the Late Mesozoic granitic rocks are of the I-type calc-alkaline series,

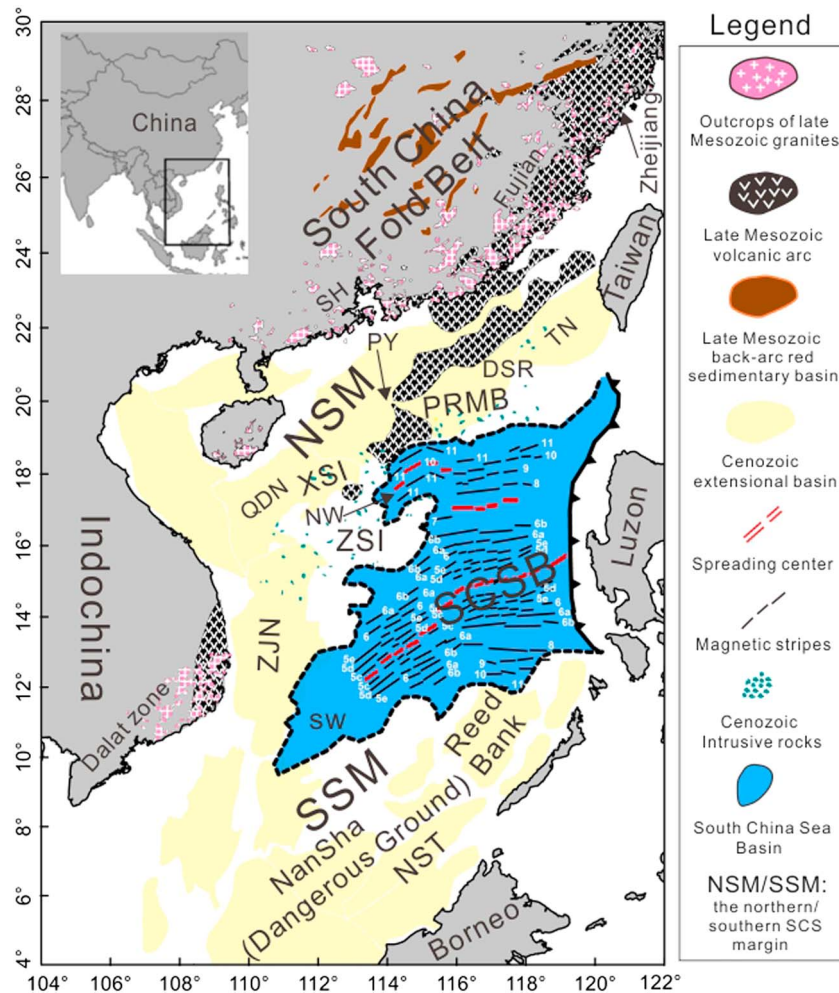


Figure 1. Schematic map for the distribution of the Late Mesozoic granites, volcanic arc and back-arc sedimentary basins in and around the SCS. NSM = northern SCS margin; SSM = southern SCS margin; SCSB = SCS basin; SW = southwest subbasin; ZSI = Zhongsha Islands (Macclesfield bank); XSI = Xisha Island (Paracel Islands); PRMB = Pearl River Mouth Basin; ZJN = Zhongjiannan Basin (Phu Khanh Basin); NST = Nansha Trough (northwest Palawan Trough); DSR = Dongsha Rise; NW = northwest subbasin; SH = Sanshui Basin; QDN = Qiongdongnan Basin; TN = Tainan Basin; PY = Panyu Low Uplift. Compiled after Hoa et al. (2008), Lan et al. (2003), Thuy et al. (2004), D. Zhou, Wang, et al. (2006), X. M. Zhou, Sun, et al. (2006), and X. Zhou and Li (2000, and references therein).

and these samples lie within the volcanic arc field on the Rb-Y and Nb-Y diagrams, similar to those from the onshore arc belt (P. L. Li, Liang, et al., 1999; Q. Yan et al., 2014). However, previous studies on the distribution of the Mesozoic volcanic arc in the northern SCS margin are mostly inferred using geophysical data, such as magnetic anomalies, due to the limited samples obtained offshore (Xia & Huang, 2004; Yao et al., 1994; D. Zhou, Wang, et al., 2006).

From the magnetic anomaly map in the northern SCS margin, a wide zone of high-amplitude positive magnetic anomaly (HPMA) starting approximately from the PRMB and extending southwestward to the Zhongsha (Macclesfield Bank) and Xisha Islands (Paracel Islands) has been clearly recognized. However, the origin of this zone has been controversial. Xia and Huang (2004) suggested that the high-amplitude zone was generated by mafic-ultramafic rocks in the lower crust. J. B. Li and Jin (2008) viewed the zone as a magmatic belt, which was formed by remelting of crust during collision between the Eurasian continental fragments and the East Asia in the Late Cretaceous. Dai (1997) interpreted this HPMA zone as one part of the onshore Mesozoic volcanism along the coast line of Fujian and Zhejiang provinces, which was then split and pulled toward southeast due to Cenozoic extension. By comparing the characteristics of the

high-amplitude zone with the Luzon island arc and the well-known Mesozoic volcanic arc in the Fujian-Zhejiang coastal line, it has also been suggested that the zone should be the Mesozoic volcanic arc (Yao et al., 1994; D. Zhou, Wang, et al., 2006).

In summary, previous analyses have shown that the HPMA zone is associated with Mesozoic magmatic activities, although the dynamics remain under debate. Whether the zone is caused by Mesozoic volcanic arc or ultramafic rocks or by the remelting of crust in the Late Cretaceous demands additional constraints, such as petrological evidence. Z. Wu et al. (2011) proposed that the belt represents the Mesozoic magmatic rocks according to the drilling samples from the Dongsha Rise, which consists of arc-signature intermediate-acidic igneous rocks. However, no further petrological effort has been used to constrain the origin of the high-amplitude belt. As more available petrologic and geochronologic data are reported, comprehensive analysis is necessary to confirm whether the high-amplitude magnetic anomaly belt is consistent with the Mesozoic volcanic arc in the northern SCS margin.

The southern SCS continental margin (e.g., the NanSha [Dangerous Grounds] and the Reed Bank) once occupied a predrift position contiguous with the South China block, having a similar geodynamic setting to the South China block in the Mesozoic era (Briais et al., 1993; Ding et al., 2013; Franke et al., 2014; Hall, 2002; Taylor & Hayes, 1983; Yao, 1996; D. Zhou et al., 2005). The southern SCS continental margin is a convergent margin with an Andean-type volcanic arc from the Jurassic to Cretaceous based on stratigraphic and tectonic evidence from the North Palawan Island (Holloway, 1982). Granite samples dredged from the Dangerous Grounds fall in the fields of arc-like area with typical I-type characteristics in the trace element and isotopic characteristics, thereby providing direct evidence for the existence of Mesozoic volcanic arc in the southern SCS margin (Q. Yan et al., 2010). However, the distribution of the Mesozoic volcanic arc in the southern SCS margin, and its relationship with that of the northern continental margin remains unclear. The best way to identify the spatial distribution of the Mesozoic volcanic arc in the south is magnetic anomaly analysis supplemented with petrological constraints using the drilled/dredged samples.

In this study, we reprocess the magnetic data to delineate the distribution of high-amplitude zones in the SCS margin. By analyzing the magnetic characteristics and newly collected petrological evidence, we further investigate whether the high-amplitude magnetic anomaly belt is consistent with the Mesozoic volcanic arc and infer the possible spatial distribution of the Mesozoic volcanic arc in the SCS margin. In addition, evidences from depositional environment and seismic profiles provide independent support to our interpretation of volcanic arc. Moreover, the tectonic implications of the Mesozoic volcanic arc to the evolution of the SCS basin are discussed.

2. Geological Setting

The SCS basin is a marginal sea located at the west of the Pacific, trending NE-SW (Figure 1). Its geological boundaries are characterized by subduction in the east, extension in the north, strike slip in the west, and collision in the south. According to the ages and directions of magnetic lineation in the basin, numerous works deduced that the SCS basins have experienced several opening episodes from 33 to 16 Ma during the Oligocene and Early Miocene (Briais et al., 1993; Hsu et al., 2004; C. F. Li, Xu, et al., 2014; Taylor & Hayes, 1983; Xu et al., 2012 etc.). Spreading first occurred in the northeast and led to the formation of the eastern subbasin of SCS at approximately 33 Ma (C. Li et al., 2015). After ~25.5 Ma, the spreading center migrated southward and the opening of the northwest SCS subbasin stopped. Since ~23 Ma, the spreading event that jumped from the north kept propagating southward, leading to the formation of the southwest subbasin of the SCS (Briais et al., 1993). As a result, the Dangerous Grounds and the Reed Bank were separated from the continental South China block, moved in the southeast direction, and finally collided with Borneo in the Middle Miocene (Clift et al., 2008; Holloway, 1982; Hutchison, 1996; Jin & Li, 2000; Taylor & Hayes, 1983).

The northern continental margin of the SCS lies between the South China Fold Belt and the continent-ocean transition (COT) and includes a series of rifted basins (e.g., Sanshui, Pearl River Mouth, Southwest Taiwan, and Qiongdongnan Basins; e.g., Clift & Lin, 2001; Hsu et al., 2004; X. Xie et al., 2006). The southern SCS continental margin is a thinned crust and has drifted from the Eurasian plate during the opening of the SCS basin (Hamilton, 1979). NE trending Cenozoic basins are widely distributed in the Dangerous Grounds, such as the Nanwei and Reed Bank Basin. A belt of NW thrust sheets developed in the Northwest Palawan Trough, which is considered to be caused by the subduction of the proto-SCS crust beneath Borneo Island (Hall,

2002; Hutchison, 2004). In the Collision-Extrusion model, instead of collision with Borneo, the Dangerous Grounds and the Reed Bank were extruded along the Red River Fault due to the collision between India and Asia (Briais et al., 1993; Cullen et al., 2010; Hall et al., 2008; Replumaz & Tapponnier, 2003; Tapponnier et al., 1990, 1986, 1982).

In the Mesozoic, the SCS basin did not exist nor did the adjacent SCS margins located at the Eurasian continental mainland (C. F. Li et al., 2008). According to the onland research, from the mid-Jurassic to Late Cretaceous, the Paleo-Pacific plate was subducting northwestward beneath the southeast Eurasian plate, and consequently, a series of NE trending Mesozoic volcanism developed (e.g., Lapierre et al., 1997; Z. X. Li & Li, 2007; Sewell & Campbell, 1997; X. Zhou & Li, 2000). Igneous rocks consist of widely exposed granites, rhyolites, gabbros, basalts, diorite, and andesite and extend from Japan through Southeast China into Southern Vietnam (Nguyen, Satir, Siebel, & Chen, 2004; Nguyen, Satir, Siebel, Vennemann, & Long, 2004; Phan, 1992).

In the Southeastern China area, the Late Mesozoic magmatism extends from Northeast China to Hainan Island, parallel to the South China coastal line. On the mid-ocean ridge basalt-normalized incompatible trace element plot, the K_1 basalts show characteristics of Nb-Ta depletion and large ion lithophile element enrichments, indicating their origin of subduction-related wet mantle wedge melting and further showing that K_1 basalts are genetically of the volcanic arc type, which are derived from active continental margin magmatism (McCulloch & Gamble, 1991; X. M. Zhou, Sun, et al., 2006). In combination with the coexisting A-type alkaline and microlitic granites, mafic and felsic dikes, previous studies have delineated the K_1 continental margin as magmatic arc systems in the coastal region of the Southeastern China, trending NE-WS (e.g., Campbell & Sewell, 1997; Jahn et al., 1976; Niu, 2005; D. Z. Wang & Zhou, 2002; F. Y. Wu et al., 2005; Q. Yan et al., 2014; X. Zhou & Li, 2000; Figure 1). In comparison, the K_2 tholeiitic basalts interlayered with red beds do not show Nb-Ta depletion, which represent the development of back-arc extensional basins in the interior of Southeast China (X. M. Zhou, Sun, et al., 2006).

In the Dalat zone of the Indochina Peninsula, Southern Vietnam, Mesozoic plutonic and contemporary volcanic rocks have been widely explored and interpreted as subduction-related products (Taylor & Hayes, 1983). Ages obtained from different radiometric methods indicate that magmatism in the Dalat zone is from the Middle to Late Cretaceous (Nguyen, Satir, Siebel, & Chen, 2004; Nguyen, Satir, Siebel, Vennemann, & Long, 2004). Moreover, granitoid samples in the zone are of I-type characteristics and low ratios of Rb/Cs, which belong to high-K calc-alkaline series, which are in favor of volcanic arc origin (Nguyen, Satir, Siebel, & Chen, 2004; Nguyen, Satir, Siebel, Vennemann, & Long, 2004). These arc-related igneous rocks, together with the Mesozoic magmatism activities in the SCS margin, comprise a continuous Andean-type volcanic arc in East Asia (Huang, 1963; Jahn et al., 1976; Z. X. Li & Li, 2007; Nguyen, Satir, Siebel, & Chen, 2004; Nguyen, Satir, Siebel, Vennemann, & Long, 2004; Taylor & Hayes, 1983).

After the Late Cretaceous, a major tectonic event terminated the Paleo-Pacific subduction. Scientists have inferred that the subducting plate encountered rollback process (Lapierre et al., 1997; Z. X. Li & Li, 2007). Following this tectonic event, the southeast Eurasian continent has transformed from active to passive continental margin. Consequently, the SCS region encompassed a broad spectrum of tectonic processes, such as rifting, seafloor spreading, subduction, and collision (e.g., Taiwan collision zone; P. Wang, 2012).

3. Data and Methods

3.1. Magnetic Data and Processing Methods

The total field magnetic data are mainly obtained from the National Oceanic and Atmospheric Administration and the Magnetic Anomaly Map of East Asia compiled by the Geological Survey of Japan (Maus et al., 2007; Maus et al., 2009). The SCS margin is located at low latitudes; hence, induced polarization is shifted laterally by inclination. Thus, the observed magnetic fields may bias their sources, making the magnetic interpretation difficult. To overcome the dipolar nature of the geomagnetic field and center the peaks of magnetic anomalies over their sources, we reprocess the total magnetic field data using the technique of variable magnetization to obtain the reduced-to-the-pole (RTP) magnetic anomalies (Figure 2). The technique of variable magnetization is derived from the Poisson's equation. Supposing that the remnant magnetization can be neglected, the gridded total field magnetic data are reduced to the pole by varying the directions

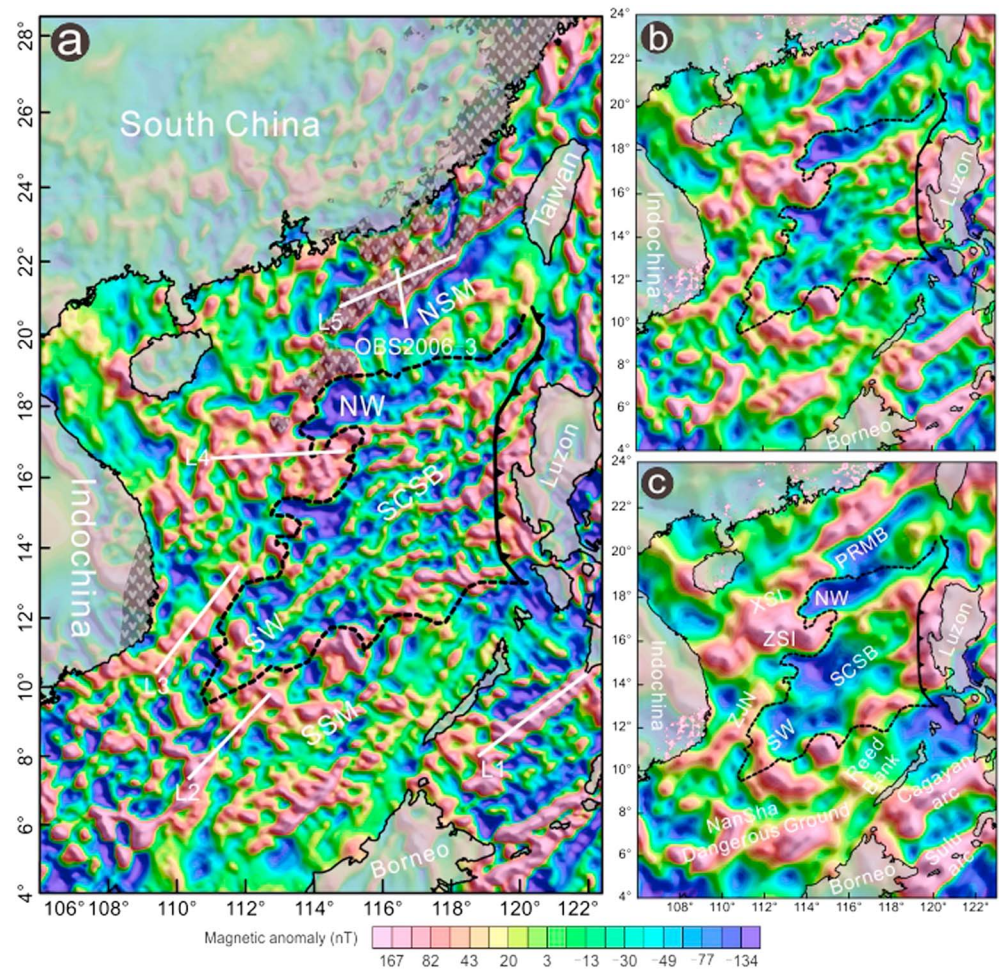


Figure 2. Map of reduced-to-the-pole magnetic anomaly (a) and upward continuation to elevation of (b) 20 and (c) 40 km for the SCS. Straight lines L1–L5 in Figure 2a are sampled profiles used to calculate their log power spectra (Figure 3), and straight line OBS2006-3 is used to conduct magnetic modeling (Figure 8). Shadow areas denote the distribution of the Late Mesozoic volcanic arc. Denotations are the same as those in Figure 1. SCSB = SCS basin; SSM = southern SCS margin; PRMB = Pearl River Mouth Basin; XSI = Xisha Island (Paracel Islands); ZJN = Zhongjiannan Basin (Phu Khanh Basin); ZSI = Zhongsha Islands (Macclesfield bank).

of magnetic inclination over the survey area. The method of variable magnetization has been already tested by synthetic and field magnetic anomaly data (L. Zhang, Zhang, & Wang, 2014). The process yields result and coincides with known source parameters.

Upward continuation of the RTP anomaly is conducted to analyze the characteristics of the magnetic anomaly. It accentuates low-frequency anomalies caused by deep sources and suppresses high-frequency anomalies due to near-surface features using fast Fourier transform technique (Blakely, 1995). Upward continuation provides a powerful tool for separating structures from different depths and obtaining the most likely geometrical shape of deep structure.

Power spectrum analysis is also conducted to determine the statistical depth to the tops of the magnetic sources. A typical power spectrum for the magnetic data consists of a deep source, shallow source component, and noise components (Figure 3). The power spectrum of the magnetic field decreases with depth to source t by an exponential factor $(-2tk)$, where k is the wave number. Thus, if the depth factor dominates the shape of the power spectrum, then the logarithmic power spectrum is directly proportional to $-2tk$, and the source depth can be calculated from the slope of the log power spectrum (Spector & Grant, 1970). The relationship between the source depth and the power spectrum can be written as

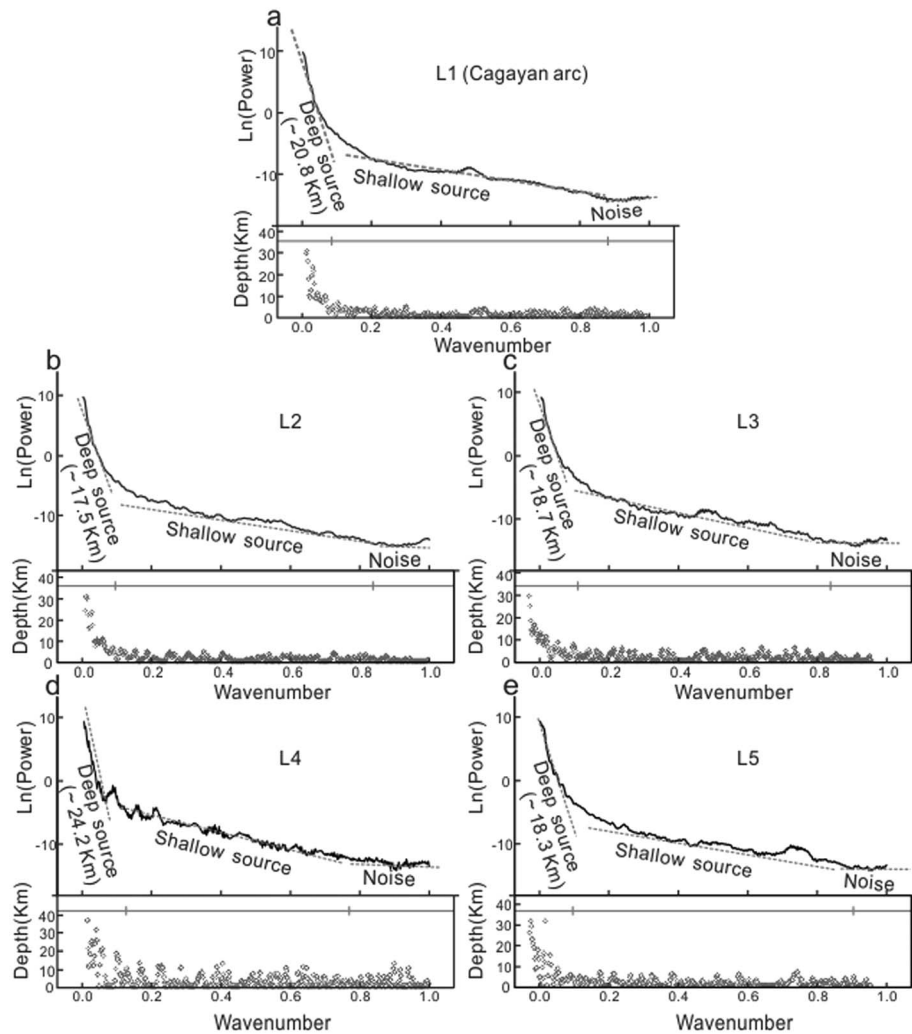


Figure 3. Power spectrum of five profiles across the high-amplitude anomaly belts. The depth estimate is a plot of the five-point depth data from the power spectrum. Locations of these profiles are shown in Figure 2a.

$$|d| = -\frac{1}{4\pi} \frac{(\log E_1 - \log E_2)}{k_1 - k_2}, \quad (1)$$

where the source depth d depends on the power spectrum (E_1, E_2) and the wave numbers (k_1, k_2).

3.2. Drilling and Dredging Data

The drilling and dredging data are collected from the China National Offshore Oil Corporation (CNOOC) and the Guangzhou Marine Geological Survey (GMGS), as well as published literature. Nearly 100 drilling boreholes have reached the pre-Cenozoic basement in the north and south of the SCS margin. The Late Mesozoic igneous rocks were also dredged from the SCS margins. These data provide important petrological evidence. More information about the samples, such as location, age, and lithology of rocks, are shown in Table 1 and Figure 4.

3.3. Seismic Data

A large number of seismic experiments have been conducted in the continental margins since 2006 by CNOOC, especially in the northern SCS. The profiles ec00-1747 and 07ns-6 have been used in this study. These profiles have been conducted with air gun volume larger than 3,000 cubic inch, and the shot point interval is 12.5 m. The data are collected by a 7.5-km-long streamer with 960 channels. The dominant

Table 1
Location, Age, and Lithology of the Mesozoic Intermediate, Agglomerate, and Felsic Rocks

No.	Well	Longitude	Latitude	Depth (m)	Age (Ma)	Lithology	Reference
1	HZ33-2-2	115.68	21.06	2,455.5	Mesozoic	Andesite	1
2	HZ27-1-1	115.48	21.29	3,052	Mesozoic	Andesite	1
3	LF13-2-1	116.15	21.56	3,280	Mesozoic	Andesite	1
4	HJ32-1-1	117.22	22.05	1,695	Mesozoic	Agglomerate	1
5	XJ34-3-1	114.5	20.96	3,296	78.5 ± 3.2	Agglomerate	1
6	BD6-1-1	111.85	18.93	2,133	87	Agglomerate	1
7	HZ25-1-1X	115.12	21.13	3,041	99.8 ± 1.53	Agglomerate	1,8
8	LH11-1-2	115.85	20.74	1,799.5	Mesozoic	Skomerite	1
9	HZ21-1-1	115.42	21.31	2,779	105	Diorite	1
10	LH21-1-1	115.36	20.43	2,779	Mesozoic	Diorite	1
11	LH19-4-1	115.14	20.33	3,068.5	Mesozoic	Diorite	1
12	PY24-1-1	114.92	20.42	4,391	42.5	Diorite	1
13	S2-1-1	112.23	19.54	3,641.2	118	Granite	8
14	AY-1X	108.47	5.62	2,811	54.6 ± 2.7	Agglomerate	7
15	28-a-1x	106.87	7.4	1,504	Pre-R	Quartz diorite	2
16	Sampaguita-1	116.52	10.44	3,353	K1	Quartz diorite	4
17	AS-1X	108.42	6.85	1,728	129 ± 7	Diorite	7
18	SO27-24	115.83	9.88	*	T2	Diorite	6
19	SO23-23	115.87	9.9	*	T3-J1	Olivine-gabbro rhyolite	6
20	DUA-1x	108.43	7.44	4013	K	Granite	2
21	DUA 12-B-1X	108.27	7.50	3889	*	Granite	2
22	15-C-1X	108.30	9.97	3,276	Pre-R	Granite	2
23	Dragonax 15C	108.36	10.42	*	Yanshanian	Granite	12
24	DH-3	108.64	8.45	*	Pre-R	Granodiorite	2
25	DH-1	108.69	8.49	3352	109 ± 5	Granite	2
26	Cipta-b	108.55	6.30	3274	Pre-R	Granodiorite	2
27	AT-1X	108.65	5.49	1768	80 ± 2.4	Biotite granite	2
28	AP-1X	109.62	5.52	4199	79.3	Granodiorite	2
29	12-C-1X	108.02	7.52	3,657	Pre-R	Granite	2
30	04-B-2X	108.92	8.63	2593	*	Volcanic rock	2
31	04-B-1X	108.99	8.63	2442	K1	Volcanic rock	2, 11
32	ZHU5	114.5	20.97	3,231	75	Granodiorite-porphry	1,8
33	LF35-1-1	116.7	21.02	1,030	K2	Rhyolite	1,3
34	YJ21-1-1	112.3	20.45	1,648–1,858	51.8 ± 8.3	Rhyolite	1
35	WC8-2-1	112.37	19.75	2,628	Mesozoic	Rhyolite porphyry	1
36	LF22-1-1	116.63	21.45	1,726	Mesozoic	Granite	1
37	HZ10-1-1	115.65	21.75	2,763	Mesozoic	Granite	1
38	HZ22-1-1	115.63	21.3	2,798.5	Mesozoic	Granite	1
39	ZHU2	114.51	21.34	2,372	70.5	Coarse grained	1,8
40	XJ24-1-1X	114.98	21.31	3,760	84	Granite	1,8
41	XJ30-2-1X	114.97	21.23	3,577	Mesozoic	Granite	1
42	XJ36-3-1X	114.9	21.1	3,725	Mesozoic	Granodiorite	1
43	HZ32-2-1	115.17	21.13	2,718	88.5 ± 3.6	Granite	1
44	HZ32-3-1	115.22	21.12	2,614	Mesozoic	Granite	1
45	HZ26-1-1	115.25	21.14	2,470.5	Mesozoic	Granite	1
46	HZ26-1-2	115.27	21.13	2,591	Mesozoic	Granite	1
47	HZ33-1-1	115.35	21.1	2,610	86.2–93.2	Granite	1
48	HZ34-1-1	115.55	21.02	2,300	Mesozoic	Granite	1
49	LH11-2-1	115.74	20.7	1,879	90.62 ± 1.49	Granite	1
50	DS7-1-1	116.11	20.64	1,333	Mesozoic	Granite	1
51	LH18-1-1	115.93	20.55	1,838	Mesozoic	Granite	1
52	LH18-2-1	115.95	20.45	1,864	Mesozoic	Granite	1
53	PY4-1-1	114.6	20.82	3,139	130.0 ± 5.0	Granite	1,8
54	PY3-1-1	114.43	20.93	3,171	90.7 ± 3.3	Granite	1,8
55	PY14-5-1	114.2	20.62	3,788	Mesozoic	Granite	1
56	PY15-1-1	114.41	20.52	4,401.5	Mesozoic	Granite	1
57	PY20-1-1	114.23	20.37	3,856	Mesozoic	Biotite granite	1
58	EP18-1-1A	113.98	20.49	3,426	100.5 ± 1.7	Granite	1
59	ZHU1	113.57	21.15	1,817.9	73.0–76.0	Coarse-grained granite	1,8
60	ZHU4	114.27	21.19	3,203.5	Mesozoic	Coarse-grained biotite	1,8

Table 1 (continued)

No.	Well	Longitude	Latitude	Depth (m)	Age (Ma)	Lithology	Reference
61	HZ35-1-1	115.69	21.05	2,212.5	105	Granite	1
62	EP25-1-1	113.14	20.25	3,164	Mesozoic	Granite	1
63	ZHU7	114.37	20.95	*	Mesozoic	Granite	1
64	HZ32-2-2	115.68	21.05	2,783.5	Mesozoic	Granite	1
65	QH36-2-1	111.85	19.13	1,251	Mesozoic	Granite	1, 11
66	XJ30-1-1X	114.95	21.2	3,152	Mesozoic	Granodiorite	1
67	LF2-1A	116.23	22.0	2,480–2,483	100.38 ± 1.46	Granite	8
68	LF13-1-1	116.04	21.60	3,193	*	Cataclastic granite	1
69	XJ17-3-1	114.69	21.50	2,122–2,124	72.98 ± 2.8	Granite	8
70	XJ24-3-1A	114.91	21.38	4,318–4,319	98	Granite	8
71	HZ25-2-1X	115.02	21.20	3,176	99.8 ± 1.53	Granite	1
72	HZ32-3-1	115.22	21.12	2,614	Mesozoic	Granite	1
73	LH1-1-1X	115.12	20.87	2,572.5	43.15 ± 0.7	Granite	1
74	LH11-1-1A	115.74	120.7	1,836.5	90.62 ± 1.49	Granite	1
75	PY21-3-1	114.38	20.42	4,018–4,019	89.83 ± 1.32	Granite	8
76	PY27-1-1	114.51	20.02	3,607–3,609	118.9 ± 2.1	Granite	8
77	KP9-1-1	113.59	19.54	1,662–1,774	153 ± 6	Granite	8
78	XiYong	112.4	16.25	1,384.6	144–158	Monzogranite Diorite	1,10
79	ZhongSha	114.57	16.21	*	126.63 ± 2.02 119.32 ± 1.91	Granite	9
80	S08-32-1	114.08	11.47	Dredging	153.6 ± 0.3	Monzogranite	5
81	S08-18-2	114.93	11.78	Dredging	159.1 ± 1.6	Tonalite	5
82	So23or27	116.58	12.1	Dredging	146	Amphibolite	5
83	HZ28-2-1	116.65	22.43	3,942–3,943.6	109.3 ± 2.4	Granite	8
84	Y26-1-1	112.25	19.98	1,700–1,702	89.2 ± 1.58	Granite	8

Note. 1. CNOOC; 2. Wu and Yang (1994); 3. Shao et al. (2007); 4. Taylor and Hayes (1980); 5. Q. Yan et al. (2008); 6. Kudrass et al. (1986); 7. Hutchison (1989); 8. P. L. Li et al. (1998); and 9. Jin (1989); 10. Xiu et al. (2016); 11. GMGS; 12. Areshev et al. (1992). All the drilling/dredging locations are shown in Figure 4. Asterisks (*) means no data available.

frequency of the signals is 75 Hz, equivalent to a vertical resolution of 8–10 m. The reflection data have been then processed by CNOOC with a standard procedure, including filtering, multiple suppressing, stacking, and time migration.

4. Results

4.1. Characteristics of Magnetic Anomalies in the SCS Margin

Figure 2a shows the map of RTP magnetic anomaly for the SCS region constructed by the methods described earlier. Inside the SCS basin, high-frequency intercalated magnetic lineations are discriminated with values up to 200 nT. At the same time, several other wide magnetic anomaly belts with amplitude up to ~220 nT are clearly delineated. Most of them correspond to well-known volcanic arcs, such as the Luzon, Cagayan, and Sulu arcs (Figure 2a). Similar to other arcs, these volcanic arcs are characterized by HPMA, which is believed to be common in subduction zones due to high magnetic susceptibility for the volcanic rocks (Kushiro, 1974; Tatsumi, 1982; D. Zhou, Wang, et al., 2006). For example, the Luzon arc shows distinct magnetic anomaly amplitude of ~220 nT (Figure 2a). Northeast to Borneo, two distinct HPMA belts striking SW-NE correspond to the Cagayan and Sulu arcs. The anomaly amplitudes of the Cagayan and Sulu arcs are similar to those of the Luzon arc. In addition to the volcanic arcs, several short HPMA belts are identified in the SCS basin. They are striking SW-NE, approximately parallel to the spreading axis, and represent the magnetic stripes in the SCS basin. Such features are consistent with those in the previous findings from the total magnetic field (C. F. Li et al., 2008, 2010).

In addition to the known features, several other prominent magnetic anomaly belts with similar amplitude to that of the Luzon, Cagayan, and Sulu arcs are discriminated. They are striking NE-SW, are distributed on both sides of the SCS basin, and do not correspond to any known structures in the region (Figure 2a). In the northern SCS continental margin, the HPMA belts cross the Panyu Low Uplift and Dongsha Uplift and extend southwestward to Zhongsha Islands. Previous studies have interpreted the belts in the northern SCS margin

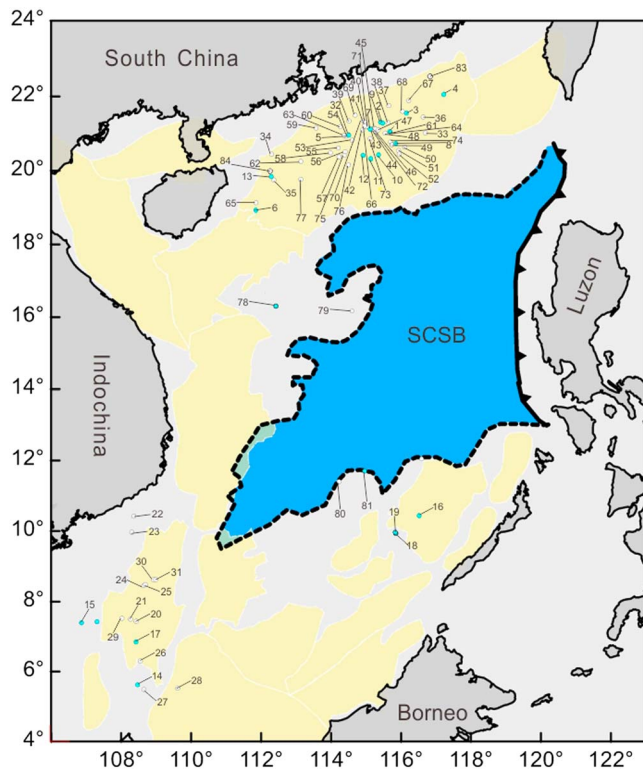


Figure 4. Locations of the drilling/dredging data in the South China Sea margin. The names for all drilling/dredging were replaced with numbers. See Table 1 for full name, longitude, latitude, age, and lithology. SCSB = South China Sea basin.

as the volcanic arc associated with Mesozoic subduction (e.g., Z. Wu et al., 2011; D. Zhou, Wang, et al., 2006). Further southwestward, several other broken positive HPMA belts are distributed around the southwest subbasin. In Comparison with the belts in the north, the anomaly amplitude in the southwest is slightly smaller and less continuous. The magnetic belts in the northern SCS margin have been interpreted as the volcanic arc associated with Mesozoic subduction. To date, no relevant interpretation on the positive high-amplitude anomalies in the southwest SCS continental margin is available.

To determine the most likely geometrical shape of the high-amplitude anomalies, we perform upward continuation of the RTP magnetic anomaly to suppress local, short-wavelength, and generally shallow source anomalies. The long-wavelength and generally deep source anomalies are well preserved after processing. For example, the distinct features of the magnetic anomalies in the SCS basin are associated with the reversal of the magnetic field during the opening of the SCS basin. Therefore, they likely originate from shallow sources (e.g., oceanic crust). From the upward continuation of the RTP magnetic anomaly by 20 and 40 km, the short-wavelength anomalies in the SCS basin and margins are significantly subdued (Figures 2b and 2c). As shown in Figure 2c, with further upward continuation of the RTP magnetic anomaly by 40 km, the short-wavelength anomalies in the SCS basin are largely removed, which indicate that these signals are indeed from shallow sources (e.g., oceanic crust). By contrast, the HPMA belts in the northern and southern SCS margins, as well as those associated with the Luzon, Cagayan, and Sulu arcs, still clearly remain with similar amplitude of ~220 nT. Therefore, these signals mostly have long wavelengths, likely caused by deep source geological bodies.

Volcanic arc magmas originate from partial melting of the overriding mantle in the subduction zone and accumulate at the continental crust interior, forming large-scale magmatic arc roots (Currie et al., 2015). For example, a thick high-velocity layer is imaged in the lower crust in the northern SCS continental shelf and viewed as a remnant arc (Wan et al., 2017). We note that previous studies also viewed the high-velocity layer as underplating during continental breakup (e.g., Kido et al., 2001; Nissen et al., 1995). However, their interpretations aimed at the high-velocity layer in the COT zone of the northeastern SCS but not the layer in the upper slope and the continental shelf (e.g., Nissen et al., 1995; P. Yan et al., 2001). The values of V_p/V_s in the continental shelf are smaller than that in the COT, also denoting a possibility of different origin. Additionally, the Cenozoic igneous rocks scatters across the COT (P. Yan et al., 2006; P. Yan & Liu, 2004; Q. Zhang, Wu, et al., 2014), while none occurs in the upper slope and shelf of the northern SCS. Another important reason is that the underplating is an important process for crustal formation because the addition of material provides a nontectonic way for the crust to grow and thicken (Thybo & Artemieva, 2013). However, there is no obvious crustal thickening in the zone of high seismic velocity (e.g., Kido et al., 2001; Nissen et al., 1995; Shi et al., 2005; P. Yan et al., 2001). To constrain the source depths of the HPMA belts, we extract raw data along five profiles from the RTP map and calculate their log power spectrum using fast Fourier transform (the lines shown in Figure 2a). Profiles 2 and 3 are in the southern SCS margin, whereas profiles 4 and 5 are in the northern SCS margin. For comparison, we also select one more profile (L1) across the Cagayan arc to obtain its log power spectrum. All of the five profiles coincide with the HPMA belts. The power spectrum curves are presented by log (power) versus the wave number. Magnetic source depths can be further estimated by calculating the slope gradient of the power spectrum curve.

The depth to a statistical ensemble of sources is determined by five-point averages of the slope of the power spectrum curve. As shown in Figure 3, three components of the power spectrum curve are calculated. Upward continuation demonstrates that the HPMA belts are associated with long wavelength. Therefore, we are only interested in the low-wave number domain, which represents approximate depths of deep magnetic sources. The results show that the average depth for the deep source of the Cagayan arc is

approximately 21 km (Figure 3a). The finding reflects that the deep magnetic source lies at a lower crustal level, coinciding with the depth of magmatic arc roots (Currie et al., 2015). Similarly, the curves from the northern and southern SCS margin have no clear difference in the magnetic frequency, and the estimated average source depths are of 18–24 km. It appears that, to the northern and southern SCS margins, the deep sources of the HPMA belts likely originate from the same geological bodies, such as the magmatic arc roots in the lower crust. Thus, the HPMA belts in the SCS margin might be remnant Mesozoic volcanic arc, which are distributed across the PRMB and extend southwestward to the Zhongsha (Macclesfield bank) and Xisha Islands (Paracel Islands) in the north. The belt is discontinuously distributed around the southwest subbasin in the south. Petrological evidence is collected to further constrain the origin of these HPMA belts.

4.2. Petrological Evidence for Constraining the Origin of HPMA Belts

In the northern SCS margin, more than 100 wells have been drilled, and the rock types include granites, granodiorites, agglomerate, andesite, diorite, skomerite, rhyolites, and metamorphic rocks (P. L. Li, Liang, et al., 1999). More than 20 of these wells encountered the pre-Cenozoic basement, thereby providing unprecedented petrologic evidence to constrain the geological features of the basement. A large portion of the basement consist of Late Mesozoic intermediate to silicic igneous rocks with ages ranging from ~153 to ~70.5 Ma, with an average of 100 Ma (e.g., HF28-2-1 dating to 109.25 Ma, EP18-1-1A dating to 100.5 Ma, and SH2-1-1 dating to 118 Ma; Table 1, and references therein). All the drilling and dredging data are collected from CNOOC and Guangzhou Marine Geological Survey, as well as published literature, as shown in Table 1 and Figure 4.

According to petrological, geochemical, and geochronological analyses, the compositional characteristics of the Late Mesozoic granites (e.g., PY4-1-1, PY27-1-1, XJ17-3-1, LF13-1-1, HF28-2-1, LH11-1-1A, XJ36-3-1X, XJ24-3-1AX, XJ24-1-1X, XJ30-1-1, HZ35-1-1, LF22-1-4, and HZ26-1-1) are dominated by I-type calc-alkaline series, and the granites lie within the volcanic arc field on the Rb-Y + Nb and Nb-Y diagrams, similar to those from island or continental marginal arcs (P. L. Li, Liang, et al., 1999; Q. Yan et al., 2014). In addition, nine boreholes (e.g., HZ33-2-2, HZ27-1-1, LF13-2-1, and XiYong-1) encountered Late Cretaceous intermediate rocks (e.g., andesite and diorite) and agglomerates. The evolution of intermediate rocks (especially andesite) has been described as derivative magma produced by the fractional crystallization of basaltic magma, which was derived by partial melting of mantle peridotite due to hydration by water released from the subducted oceanic plate (And & Kinzler, 2014; Fitton, 1971; Marsh & Carmichael, 1974). Agglomerates are igneous rocks that are ejected during explosive volcanic eruptions and are usually stored well in situ (McBirney, 1980). Therefore, the intermediate rocks and agglomerates are usually regarded as an indicator of volcanic arc.

The southern SCS margin, which drifted from the South China block during the opening of the SCS in the Cenozoic, has similar geodynamic setting to the Southeastern China and the northern SCS margin during the Mesozoic (Hall, 2002). Several samples drilled/dredged from the southern SCS margin contain granites, tonalite, monzogranite, rhyolite, diorite, and amphibolite with ages of the Late Mesozoic (Kudrass et al., 1986; Q. Yan et al., 2008). The dating results are consistent with those for Late Mesozoic igneous activities in the PRMB and Eastern China (John, 1990; X. H. Li, 2000; Z. X. Li & Li, 2007; F. Y. Wu et al., 2005; X. Zhou & Li, 2000). Intermediate rock and agglomerate obtained from SO27-24, AS-1X, AY-1X, 28-a-1x, and Sampaguaita-1 support the existence of Mesozoic volcanic arc in the southern SCS margin. More details, including sampling location, lithology, and geochronology of rock samples, are listed in Table 1. Meanwhile, granitic samples from SO8-18 and SO8-32 are plotted in the fields of arc-like signature with typical I-type characteristics by applying trace element and isotopic characteristic analysis (Q. Yan et al., 2010).

The temporal-spatial distribution of Mesozoic arc-like signature granites, intermediate rocks, and agglomerates in the SCS margin is summarized in Figure 5. Most of these rocks are distributed in the northern SCS margin and coincide with the HPMA belts, supporting that the belts in the north originated from the existence of Mesozoic volcanic arc. In the southern SCS margin, small and less continuous belts are also consistent with the petrologic evidence, except the belts in the Zhongjiannan Basin (Phu Khanh Basin) and the Nansha Trough (NW Palawan Trough). Although these two belts have not been verified due to the lack of drilled/dredged samples, we also infer that the two belts are caused by Mesozoic volcanic arc because they have similar geophysical characteristics to others. Of course, our interpretation on the two belts should be further confirmed in the future if more drilling/dredging data are available. Based on aforementioned analysis, we suggest that the source of the HPMA belts in the SCS margin is of Mesozoic volcanic magmatism.

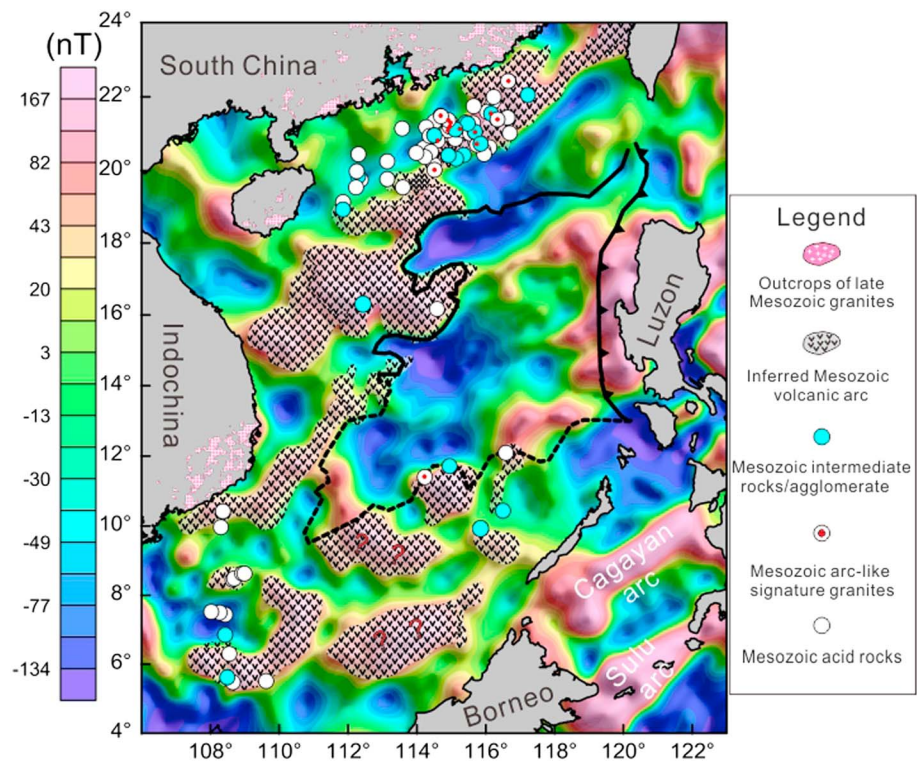


Figure 5. Map showing the possible spatial distribution of Mesozoic volcanic arc in the present-day South China Sea margin according to the Late Mesozoic igneous rocks and reduced-to-the-pole magnetic anomaly upward continued to 40 km.

4.3. Additional Evidence From the Mesozoic Depositional Environment and Seismic Interpretation

The well LF35-1-1 was drilled in the Chaoshan Depression, northern SCS margin. The 2,187- to 2,388-m interval of well LF35-1-1 contains a dominant combination of *Cyathdites* and *Classopollis*, which are two of the most unusual fossil pollen types and indicate a shallow-water shelf environment (G. X. Wu et al., 2007; G. Q. Xu et al., 2013). These two fossil pollens were widely distributed in middle Jurassic deposits and died out at the beginning of the Paleogene, indicating an age of Middle Jurassic (Vakhrameyev, 1983). During the Late Jurassic, the northern SCS margin was in a deep-sea environment where radiolarians and silicious radiolarian mudstone was developed in the 1,725- to 1,887-m interval of LF35-1-1, with ages dating to the Late Jurassic to Early Cretaceous (G. X. Wu et al., 2007; G. Q. Xu et al., 2013). These results suggest that parts of the northern SCS continental margin has transformed from shallow-water depositional environment to deep-sea environment around the Middle Jurassic and back to shallow-water till terrestrial in the Late Cretaceous (Shao et al., 2007). In addition, at least 18 marine and transitional clastic samples with ages of Late Jurassic to Early Cretaceous were encountered in the Tainan basin (D. Zhou, 2002). In combination with the interpretation of seismic profiles, previous studies delineated the distribution of Late Jurassic to Early Cretaceous marine facies in the northern SCS margin, which extends from Taiwan and westward to Chaoshan Depression and Dongsha Uplift (P. L. Li et al., 1998; D. Zhou et al., 2004; Figure 6). Furthermore, an early Late Cretaceous Yuli high-pressure and low-temperature metamorphic belt filled by marine facies was found across the central Taiwan orogeny. The belt consists of black and green schists and originates from trench-fill turbidites, basalts, and basaltic tuff (Beyssac et al., 2007; Ho, 1986). This finding suggests that the belt and/or part of the marine facies strata are possibly the result of the accretion of oceanic material (Jahn et al., 1986).

In the Reed Bank and Dangerous Grounds, the Lower Cretaceous neritic clastic rocks (e.g., sandstone and siltstone) have been found in the Sampaguita-1 (Taylor & Hayes, 1980), Sampaguita-2, Sampaguita-3, Kalamansi-1, Reed Bank-A1 (Schlüter et al., 1996a), and Reed Bank-3A (Soeparjadi et al., 1985), indicating a typical neritic depositional environment for the southern SCS continent in Mesozoic (Figure 6). Meantime, Sales et al. (1997) concluded that the Early Cretaceous to Jurassic marine facies was widely distributed in

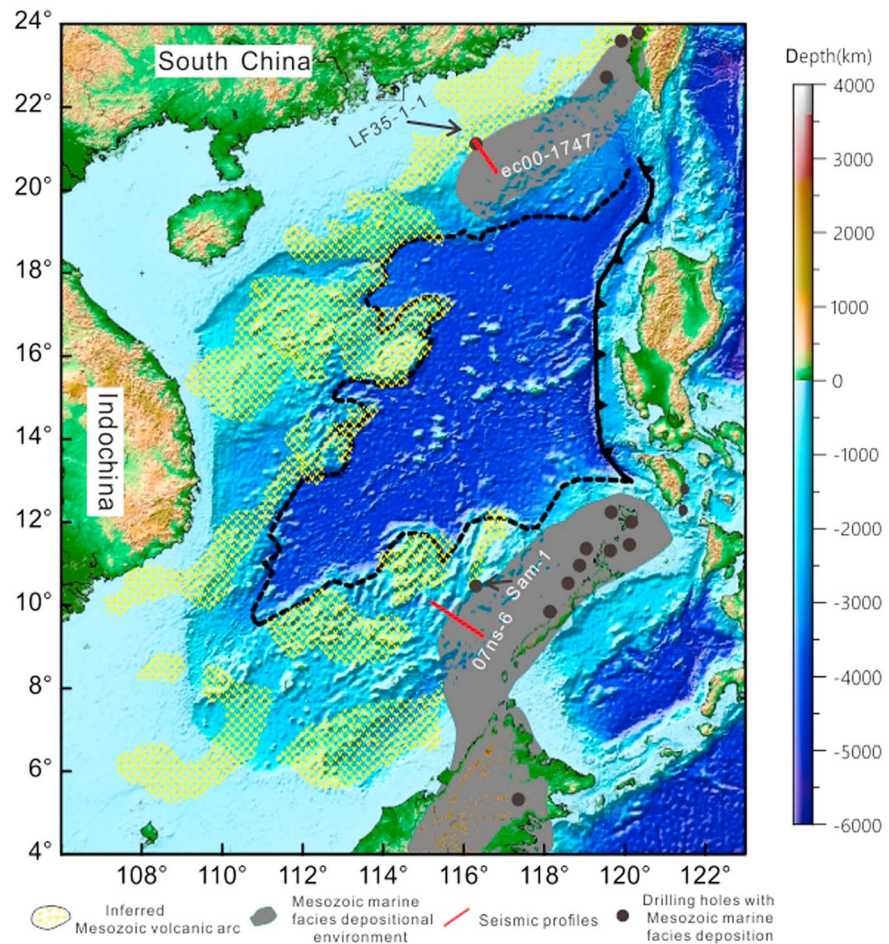


Figure 6. Schematic plot showing the distribution of Mesozoic volcanic arc and marine facies in the South China Sea continental margin (modified after Chen et al., 2003; G. X. Wu et al., 2007; P. Yan & Liu, 2004; D. Zhou et al., 2004).

the Reed Bank based on the drilling-confined seismic profile interpretation (Figure 6). A belt of Mesozoic subduction-accretion complexes exists in the North Palawan and Calamian Island and mainly consists of cherts and turbidites (Isozaki et al., 1988; Marquez et al., 2006; Tumanda, 1991). Combining with the distribution of Mesozoic subduction-accretion complexes belt, the Early Cretaceous to Jurassic marine facies (including neritic depositional environment) may represent an accretion process in the Late Mesozoic, which is considered to be related to the Paleo-Pacific subduction (Yumul, 2007; D. Zhou et al., 2008).

Seismic profiles collected from CNOOC and literature indicate a compression environment in the area of marine facies in the Late Mesozoic. For example, profile ec00-1747 crosses the drilling well LF35-1-1 in the northern SCS margin (Figure 6), and the Tg interface is viewed as the boundary between the Cenozoic and Mesozoic strata with an age of approximately 65 Ma. Below Tg, well-developed Mesozoic strata are found. Scientists have discriminated several paleosequence boundaries, such as Tm18, Tm20 (K₂), Tm30 (K₁), Tm60 (J₁), and Tm80 (T₃) constrained by well LF35-1-1 (Figure 7a). The Mesozoic strata are clearly folded with several thrust faults cutting through the sequence boundaries Tm30, Tm60, and Tm80, indicating that the stress regime was compressive during the Mesozoic Era (e.g., C. F. Li et al., 2008; Q. Yan et al., 2014). Another seismic reflection profile 07ns-6 is also found across the Reed Bank (Figure 7b). The boundary between Cenozoic and Mesozoic, Tg, and several Mesozoic sequence boundaries is clearly identified along this profile. In addition, pre-Cenozoic compressive anticlines and thrust faults are identified beneath Tg (M. Zhou et al., 2013).

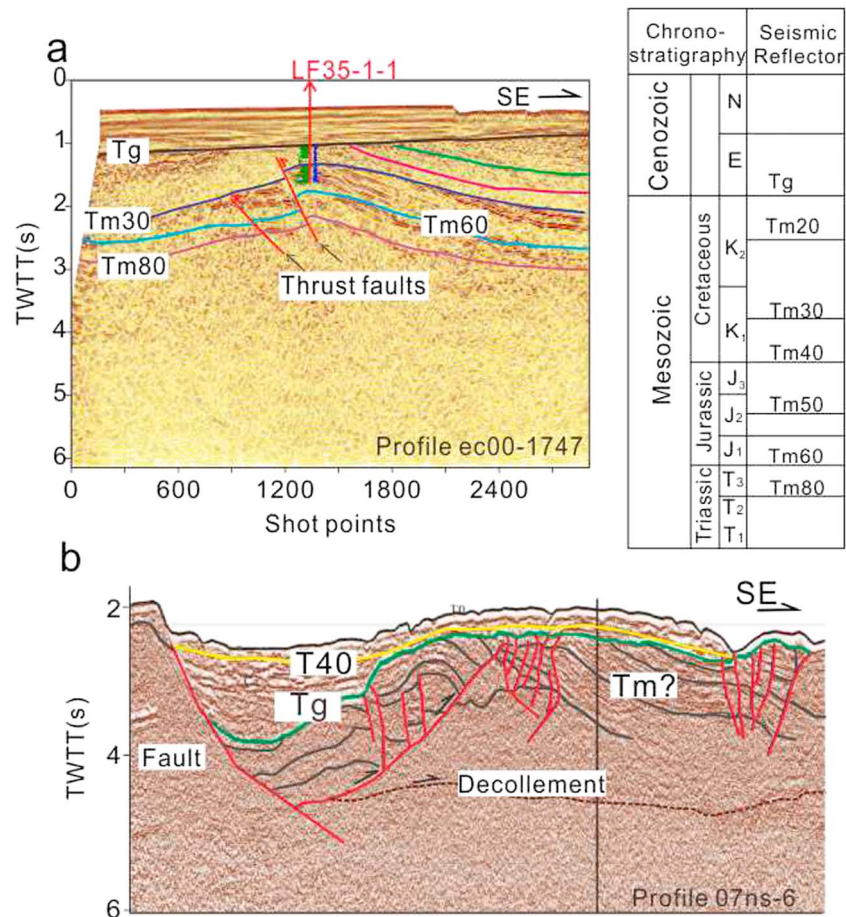


Figure 7. Seismic profiles (a) ec00-1747 and (b) 07ns-6, with a simplified stratigraphic sequence scheme of Chaoshan Depression listed in the right of the profile (modified after Shao et al., 2007; M. S. Zhao et al., 2012; J. Zhang, Sun, et al., 2014; C. F. Li et al., 2008 and the data of the CNOOC). The location of the drilling well LF35-1-1 is shown on the profile ec00-1747. TWTT = two-way travel time. See Figure 6 for its location.

5. Discussion

5.1. Possible Spatial Distribution of the Mesozoic Volcanic Arc and Its Tectonic Implications

In this study, comprehensive analysis work has been conducted to delineate the distribution of Mesozoic volcanic arc in the present-day SCS margin. One of the most important evidences is the HPMA belt (Figure 2a). High magnetic anomalies over the continental margins are most likely caused by the induced magnetization of the volcanic arc, intrusive rocks, and/or serpentinized mantle rocks (Arkani-Hamed, 1988; Blakely et al., 2005). In the northern SCS margin, Cenozoic synrift and postspreading igneous intrusion occurred on an extremely small scale, and these rocks are scattered across the COT zone (P. Yan et al., 2006; P. Yan & Liu, 2004; Q. Zhang, Wu, et al., 2014; Figure 1). Thus, rifting-induced magnetic anomalies should be small scale, high frequency, and isolated. However, in the northern SCS margin there develops broad and intense anomaly belts. The contribution from the intrusive rocks is insufficient to generate these prominent magnetic patterns. Moreover, the belts concentrate along the upper slope of the northern SCS margin do not correlate with the location of intrusive rocks. In addition, the high-frequency anomalies caused by synrift and postspreading igneous intrusion are removed after upward continuation to 40 km. The signals preserved in the Figure 2c are thus low frequency. The results from power spectrum show that the low-frequency signals likely originate from the lower crust. Therefore, the anomalies in Figure 2c are not related to recent intrusive rocks. For the possibility of serpentinized mantle rocks, petrologic models suggest that serpentinized mantle rocks are consequences of hydration (Lundin & Doré, 2011). In the SCS margin, although the throughgoing crustal faults extend downward into the Moho unconformity in the COT (e.g., Dong et al., 2014; Hayes

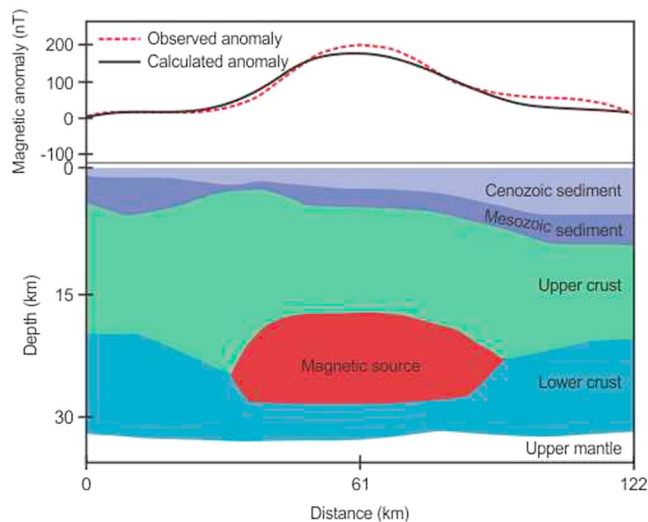


Figure 8. Magnetic modeling along the OBS2006-3 profile. See Figure 2a for its location.

et al., 1995; Y. Zhao et al., 2018), the upper slope and the continental shelf are characterized by a series of dense faults with northward dip only offset the basement (e.g., Dong et al., 2014; Y. Zhao et al., 2018). The average crustal thickness of the slope is larger than 20 km, which makes it difficult for water to arrive at the mantle. Such conditions are not conducive to the formation of serpentinized mantle rocks. Moreover, there is no evidence for the exhumation and exposure, or near exposure, of serpentinized continental mantle lithosphere on the slope. For these reasons, the effect of serpentinized mantle rocks is not considered in this study. Therefore, the sources of the HPMA belts most likely originate from the Mesozoic volcanic arc.

The average source depths for the magmatic arc are well consistent with the results imaged by deep seismic profiles (Wan et al., 2017). Previous studies have developed general models for the vertical integral of magnetization along the crustal section by assigning constant magnetization values to the magnetic crust (Mayhew et al., 1991). The results show that the lower crust may be more magnetic than the upper crust but not considerably (Mayhew et al., 1991). As such, our estimated roots of the volcanic arc may have a strong magnetization and can be

viewed as the possible sources of the anomalies. To test whether the source depths can induce the corresponding anomaly, we further conducted magnetic modeling along a profile across the HPMA belt. Deep seismic studies have already estimated the deep structure and geometry of this profile (Wei et al., 2011). On the basis of magnetic susceptibility measurements of samples from the northern SCS margin, the susceptibility of sedimentary rocks varies between 0 and 100×10^{-6} SI units, which are nonmagnetic or extremely weakly magnetic (Hao et al., 2009; Lang et al., 2011; Ubangoh et al., 2005). Based on above information, we assign a constant magnetization to each block. The values for sediment, upper crust, lower crust, and magmatic body are 0, 3, 4, and 9×10^{-1} A/m, respectively (Hao et al., 2011; Hu et al., 2008). The boundary effect is removed by extending the model domain outward by 200 km on each side. As shown in Figure 8, the major magmatic body extends 60 km laterally at the depths of 18–24 km in a direction consistent with the spatial variations of the observed magnetic anomaly. Therefore, the magnetic field of such a body can produce the amplitude of the observed anomaly.

In comparison with previous studies, our interpretation on the northern SCS margin is constrained by more pieces of petrological evidence. The results confirm that the high-amplitude magnetic anomaly belt in the north corresponds well to the Mesozoic volcanic arc. We also identify the spatial distribution of the Mesozoic volcanic arc in the south by analyzing the magnetic characteristics and newly collected petrological evidence. From the reconstruction results, we infer that the southwest part of the Mesozoic volcanic arc distributes on both sides of the southwest SCS subbasin, whereas the northeast part remains nearly in its original location, crossing the central PRMB and extending southwestward to the Zhongsha (Macclesfield Bank) and Xisha Islands (Paracel Islands; Figure 9a). Although the result can be further validated by more pieces of evidence, it is by far the most comprehensive work to answer how the Mesozoic volcanic arc distributes in the present-day SCS continental margin.

In view of the Cenozoic tectonic evolution, the spatial distribution of Mesozoic volcanic arc has been disturbed by the breakup of the SCS margin in the Cenozoic. Two conjugate patterns have been proposed to explain the drifting of the southern continental margin from the South China block. Taylor and Hayes (1983) and Franke et al. (2008) suggested that the Reed Bank on the southern SCS margin and the PRMB on the northern SCS margin are conjugate margins according to spreading direction perpendicular to the spreading center (Figure 9a). Alternately, the Reed Bank may be connected to the Zhongsha (Macclesfield Bank) and Xisha Islands (Paracel Islands) based on breakup unconformity and crustal structure (C. F. Li et al., 2014; Z. Sun et al., 2009; Qiu et al., 2011). To join the scattered Mesozoic arc together, we close the southwest, northwest, and east subsea basins following the two conjugate patterns (Figures 9b and 9c). The results showed that if we move the Reed Bank back to the PRMB, several parts of separated volcanic arc moved away from their original locations and lied within the forearc area abruptly (Figure 9b). By definition the arc rocks cannot lie within the forearc, so the Reed Bank may not connect with the PRMB

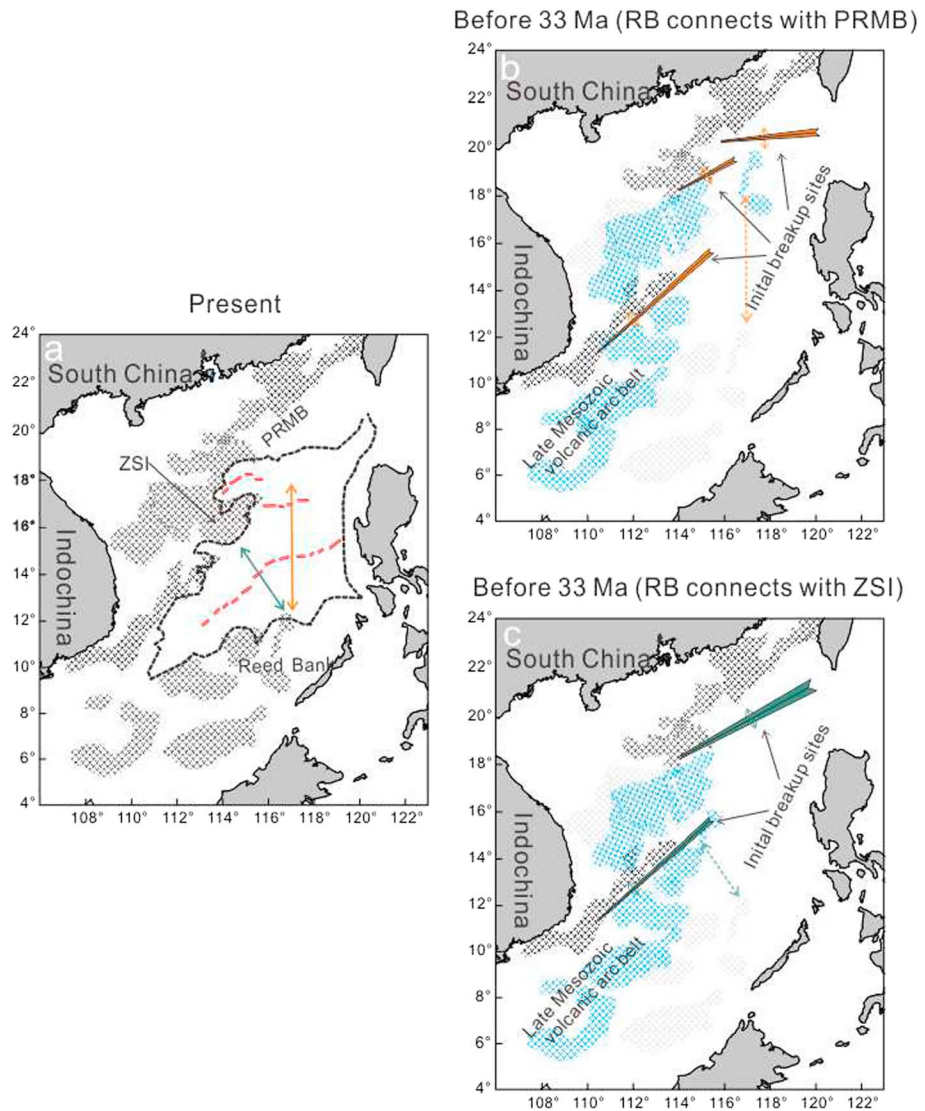


Figure 9. Models for the distribution of the Late Mesozoic arc at (a) present and (b, c) before opening of the South China Sea basin. Two different conjugate patterns are shown in green and yellow double-headed arrows. Figure 9b shows the results of joining the Reed Bank and the PRMB, and Figure 9c shows the result of joining the Reed Bank and the Zhongsha (Macclesfield Bank; ZS Ids). Denotations are the same as those in Figure 1. RB = Reed Bank; PRMB = Pearl River Mouth Basin.

before breakup. On the other hand, if we move the Reed Bank back to the Zhongsha (Macclesfield Bank) and Xisha Islands (Paracel Islands), the scattered Mesozoic volcanic arc joined well and trend NE-SW. The joined arc is parallel with the volcanic arc belt onshore and has shape similar to that of the conclusion of Morley (2012) and Taylor and Hayes (1983; Figures 1 and 9c), who used the terrestrial arc-related magmatism to infer the distribution of the Mesozoic arc. These well support that the Reed Bank is connected with the Zhongsha (Macclesfield Bank) and Xisha Islands (Paracel Islands) before breakup, which is on the other side of the southwest subbasin.

By comparing the distribution of Mesozoic volcanic arc in present-day SCS margin and before 33 Ma, it is natural to infer that the southwest part of the Mesozoic arc has been split by the spreading of the southwest subbasin, which retains the northern half along the northern boundary of the southwest subsea basin, whereas the southern half is located along the southern boundary of the sea basin and near the Dangerous Ground, as well as the Reed Bank (Figure 9c). The arcs may have been stretched and/or broken into segments during the opening of the southwest subbasin and moved southward to Borneo with the

Dangerous Ground and Reed Bank. Therefore, the process may produce less continuous magnetic anomaly as observed in our study. By contrast, the northeastern part of the Mesozoic arc remains nearly in its original location, although slightly bit stretched, suggesting that the opening of the SCS basin occurred south of the Mesozoic arc (e.g., forearc zone). Generally, the forearc spans over 250 km in width, such as the Sumatra and Mariana forearcs (Noda, 2016; Stern & Smoot, 1998). The Mesozoic forearc zone in the SCS margin has been stretched dramatically since the Oligocene, and its width has been increased accordingly. During the opening of SCS, the forearc extends over a large scale and eventually breaks apart. As the extension proceeds, the southern half of the forearc continues to drift southward, forming the present-day north Palawan block. The north Palawan block, characterized by juxtaposed chert-clastic sequences and limestone blocks in an imbricate manner, features the off-scrape accretion of oceanic sediments from the subduction of Paleo-Pacific plate during Jurassic-Early Cretaceous (Holloway, 1982; Maruyama et al., 1997; Zamoras & Matsuoka, 2004). Similar to the implication from our model, plate tectonic reconstruction also demonstrates that the opening of the SCS basin pushed the forearc-related north Palawan block southward from the northeast SCS margin, and this southbound migration ceased during the Middle Miocene when it collided with the Philippine Island arc (Holloway, 1982; Zamoras & Matsuoka, 2004).

Hence, the locus of breakup may differ in the southwest and northeast SCS continental margins during the opening of the SCS basin. In other words, the SCS basin has been formed by breaking the arc area in the southwest and forearc area in the northeast.

5.2. Favorable Conditions for the Varied Initial Breakup Sites in the SCS Margin

Similar to the Vanuatu rifting system (Maillet et al., 1995), the SCS margin also has a varied breakup locus, breaking forearc in the northeast and then propagating into the volcanic arc in the southwest. It is easy to start a rift along the arc because the arc itself generally show characteristics of heat, melt, and locally thickened crust due to the continuous magmatism upwelling and corner flow, all of which reduce the lithospheric strength (Kusznir & Park, 1987). Development of rift along the arc area is also very common in nature. For example, the Miocene Mariana volcanic arc has been split into two parts, the currently active Mariana arc and the inactive West Mariana Ridge, which are separated by the Mariana Trough (e.g., Stern et al., 2003). Similarly, in the SCS margin, a rheologically weak zone can be expected beneath the belt of the Late Mesozoic volcanic arc, reducing the rheological strength of lithosphere (Ferno & Brian, 2006) and further attracting strain localization and onset of failure during the Cenozoic extension (Kogan et al., 2012). Although a number of hypotheses have been proposed for the Cenozoic extensional force (e.g., Briais et al., 1993; Cullen et al., 2010; Lei et al., 2009; Stern & Bloomer, 1992; Tapponnier et al., 1982), they do not prevent the Mesozoic volcanic arc from being a preferential breakup site during the Cenozoic rifting.

Initial breakup can also occur within the forearc when a corner flow migrates beneath the vicinity of forearc, where the yield strength of the lithosphere decreases due to continuous heating (Ferno & Brian, 2006). The possibility of forearc breakup can be enhanced in many cases, especially if a preexisting tectonically weak zone is present because the weak zone is effective to localize deformation (Kogan et al., 2012; Li et al., 2018). In the northeastern SCS continental margin, several strong reflectors are recognized in the COT of the East Sub-Sea Basin according to deep seismic studies and analysis of geophysical characteristics (Ding & Li, 2011; Huang et al., 2005; Schlüter et al., 1996a). These reflectors are interpreted as deep-rooted faults (throughgoing faults) and formed by extension during the rollback of the Paleo-Pacific in the Late Jurassic (Lu et al., 2015). Most of the faults strike NE-NEE, dipping into the Moho and tending to weaken the continental margin (Dong et al., 2014; Franke et al., 2011). Thereby, the fractured forearc in the northeast SCS margin is easily evolved into the favored site of the initial breakup. In contrast, although complicated fault systems existed in the northwest SCS margin, these faults are mainly activated from 40 to 23 Ma and did not cut through the entire crust (Y. Xie et al., 2015). Beyond that, Pre-Cenozoic tectonically weak zone has not yet been reported in northwest. As such, the forearc in the northeast SCS margin is more likely to break up than that in the northwest.

6. Conclusions

In summary, we conduct a comprehensive analysis to infer the possible distribution of the Mesozoic volcanic arc in the SCS continental margin using petrological evidence, magnetic anomaly, data of depositional environment, and seismic profiles. Our results show that the southwest part of the Mesozoic volcanic arc is

distributed on both sides of the southwest SCS subbasin, whereas the northeast part remains nearly in its original location, which indicate that the initial sites of breakup for the northeast and southwest SCS continental margin may vary during the opening of the SCS basin. The results help us not only infer that the opening of the SCS basins has broken the arc area in the southwest and the forearc area in the northeast but also solve the puzzle of the conjugate pattern of the continental margins around the SCS.

Acknowledgments

We thank Yongjian Yao from Guangzhou Marine Geological Survey and Shuhui Chen from China National Offshore Oil Corporation for providing the drilling data. This work is supported by the joint foundation of NSFC and Guangdong province (Project U1301233), the NSFC project (41606073), the Guangdong NSF research team project (2017A030312002), and the Open Fund of the Key Laboratory of Marine Geology and Environment, Chinese Academy of Sciences (MGE2016KG03), the Strategic Priority Research Program of the Chinese Academy of Science (XDA13010303), and the Open Foundation of Key Laboratory of Submarine Geosciences, SOA. H. Yang is supported by Faculty of Science from the Chinese University of Hong Kong and HKSAR Research Grant Council Grants (24601515 and 14313816). Drilling and dredging data have been present in Table 1. For magnetic data and seismic profiles accessibility, please contact Fucheng Li (lfc@scsio.ac.cn). File types for the magnetic data and seismic profiles are grid and jpg format, respectively.

References

- And, T. L. G., & Kinzler, R. J. (2014). Petrogenesis of andesites. *Annual Review of Earth and Planetary Sciences*, 14(14), 417–454.
- Areshev, E. G., Dong, T. L., San, N. T., & Shnip, O. A. (1992). Reservoirs in fractured basement on the continental shelf of southern Vietnam. *Journal of Petroleum Geology*, 15(4), 451–464.
- Arkani-Hamed, J. (1988). Differential reduction-to-the-pole of regional magnetic anomalies. *Geophysics*, 53(12), 1592–1600. <https://doi.org/10.1190/1.1442441>
- Beysac, O., Simoes, M., Avouac, J. P., Farley, K. A., Chen, Y. G., Chan, Y. C., & Goffé, B. (2007). Late Cenozoic metamorphic evolution and exhumation of Taiwan. *Tectonics*, 26, TC6001. <https://doi.org/10.1029/2006TC002064>
- Blakely, R. J. (1995). *Potential theory in gravity and magnetic applications* (p. 461). New York: Cambridge University Press.
- Blakely, R. J., Brocher, T. M., & Wells, R. E. (2005). Subduction-zone magnetic anomalies and implications for hydrated forearc mantle. *Geology*, 33(6), 445–448.
- Briaies, A., Patriat, P., & Tapponnier, P. (1993). Updated interpretation of magnetic anomalies and seafloor spreading stages in the South China Sea: Implications for the Tertiary tectonics of Southeast Asia. *Journal of Geophysical Research*, 98, 6299–6328. <https://doi.org/10.1029/92jb02280>
- Campbell, S. D. G., & Sewell, R. J. (1997). Structural control and tectonic setting of Mesozoic volcanism in Hong Kong. *Journal of the Geological Society, London*, 154(6), 1039–1052. <https://doi.org/10.1144/gsjgs.154.6.1039>
- Chen, H. Z., Sun, Z. H., & Zhou, D. (2003). Distribution of Mesozoic lithofacies and marine strata in South China. *Journal of Tropical Oceanography (in Chinese)*, 22, 74–82.
- Chen, J., & Jahn, B. M. (1998). Crustal evolution of southeastern China: Nd and Sr isotopic evidence. *Tectonophysics*, 284(1–2), 101–133. [https://doi.org/10.1016/S0040-1951\(97\)00186-8](https://doi.org/10.1016/S0040-1951(97)00186-8)
- Chen, S., Li, Z., & Zou, Y. (1987). Major oil accumulation characteristics and exploration direction in the Pearl River Mouth Basin. *China Oil (in Chinese)*, 4(4), 12–23.
- Clift, P., & Lin, J. (2001). Preferential mantle lithospheric extension under the South China margin. *Marine and Petroleum Geology*, 18(8), 929–945. [https://doi.org/10.1016/S0264-8172\(01\)00037-X](https://doi.org/10.1016/S0264-8172(01)00037-X)
- Clift, P. D., Lee, G. H., Nguyen, A. D., Barckhausen, U., Hoang, V. L., & Sun, Z. (2008). Seismic evidence for a Dangerous Grounds mini-plate: No extrusion origin for the South China Sea. *Tectonics*, 27, TC3008. <https://doi.org/10.1029/2007TC002216>
- Cullen, A., Reemst, P., Henstra, G., Gozzard, S., & Ray, A. (2010). Rifting of the South China Sea: New perspectives. *Petroleum Geoscience*, 16(3), 273–282. <https://doi.org/10.1144/1354-079309-908>
- Currie, C. A., Ducea, M. N., DeCelles, P. G., & Beaumont, C. (2015). Geodynamic models of cordilleran orogens: Gravitational instability of magmatic arc roots. *Geological Society of America Memoirs*, 212, 1–22.
- Dai, Q. F. (1997). Analysis of magnetic field of China seas and adjacent regions. *Marine Geology and Quaternary geology (in Chinese)*, 17(2), 63–72.
- Ding, W., Franke, D., Li, J., & Steuer, S. (2013). Seismic stratigraphy and tectonic structure from a composite multi-channel seismic profile across the entire Dangerous Grounds, South China Sea. *Tectonophysics*, 582, 162–176. <https://doi.org/10.1016/j.tecto.2012.09.026>
- Ding, W. W., & Li, J. B. (2011). Seismic stratigraphy, tectonic structure and extension factors across the dangerous grounds: Evidence from two regional multi-channel seismic profiles. *Chinese Journal of Geophysics*, 54(6), 921–941. <https://doi.org/10.1002/cjg2.1674>
- Dong, D. D., Shiguo, W. U., Jiabiao, L. I., & Lüdmann, T. (2014). Tectonic contrast between the conjugate margins of the South China Sea and the implication for the differential extensional model. *Science in China Series D*, 57(6), 1415–1426. <https://doi.org/10.1007/s11430-013-4740-0>
- Ferno, M., & Brian, T. (2006). *Modes of crustal accretion in back-arc basins: Inferences from the Lau Basin* (pp. 5–30). Washington, DC: American Geophysical Union.
- Fitton, J. (1971). The generation of magmas in island arcs. *Earth and Planetary Science Letters*, 11(1-5), 63–67. [https://doi.org/10.1016/0012-821X\(71\)90140-3](https://doi.org/10.1016/0012-821X(71)90140-3)
- Franke, D., Barckhausen, U., Baristean, N., Engels, M., Ladage, S., Lutz, R., et al. (2011). The continent-ocean transition at the southeastern margin of the South China Sea. *Marine and Petroleum Geology*, 28(6), 1187–1204. <https://doi.org/10.1016/j.marpetgeo.2011.01.004>
- Franke, D., Barckhausen, U., Heyde, I., Tingay, M., & Ramli, N. (2008). Seismic images of a collision zone offshore NW Sabah/Borneo. *Marine and Petroleum Geology*, 25(7), 606–624. <https://doi.org/10.1016/j.marpetgeo.2007.11.004>
- Franke, D., Savva, D., Pubellier, M., Steuer, S., Mouly, B., Auxietre, J. L., et al. (2014). The final rifting evolution in the South China Sea. *Marine and Petroleum Geology*, 58, 704–720. <https://doi.org/10.1016/j.marpetgeo.2013.11.020>
- Gilder, S. A., Gill, J., Coe, R. S., Zhao, X., Liu, Z., Wang, G., et al. (1996). Isotopic and paleomagnetic constraints on the Mesozoic tectonic evolution of South China. *Journal of Geophysical Research*, 101, 16,137–16,154. <https://doi.org/10.1029/96JB00662>
- Gong, Z. S., Li, S. T., Xie, T. J., Zhang, Q. M., Xu, S. C., Xia, K. Y., & Liu, L. H. (1997). *Continental margin basin analysis and hydrocarbon accumulation of the northern South China Sea*. Beijing: Science China Press (in Chinese).
- Hall, R. (2002). Cenozoic geological and plate tectonic evolution of SE Asia and the SW Pacific: Computer-based reconstructions, model and animations. *Journal of Asian Earth Sciences*, 20(4), 353–431. [https://doi.org/10.1016/S1367-9120\(01\)00069-4](https://doi.org/10.1016/S1367-9120(01)00069-4)
- Hall, R., Hattum, M. W. A. V., & Spakman, W. (2008). Impact of India-Asia collision on SE Asia: The record in Borneo. *Tectonophysics*, 451(1-4), 366–389. <https://doi.org/10.1016/j.tecto.2007.11.058>
- Hamilton, W. B. (1979). *Tectonics of the Indonesian region*. Washington, DC: U.S. Government Publishing Office.
- Hao, T. Y., Xu, Y., Sun, F. L., You, Q. Y., Lü, C. C., Huang, S., & Zhao, M. H. (2011). Integrated geophysical research on the tectonic attribute of conjugate continental margins of South China Sea. *Chinese Journal of Geophysics*, 54(6), 988–1008. <https://doi.org/10.1002/cjg2.1679>
- Hao, T. Y., Xu, Y., Zhao, B. M., Zhang, Y. J., & Peng, L. L. (2009). Geophysical research on distribution features of magnetic basements in the South China Sea. *Chinese Journal of Geophysics*, 52(11), 2763–2774.
- Hayes, D. E., Nissen, S. S., Buhl, P., Diebold, J., Yao, B., Zeng, W., & Chen, Y. (1995). Throughgoing crustal faults along the northern margin of the South China Sea and their role in crustal extension. *Journal of Geophysical Research*, 100, 22,435–22,446. <https://doi.org/10.1029/95JB01867>

- Ho, C. S. (1986). A synthesis of the geologic evolution of Taiwan. *Tectonophysics*, *125*(1–3), 1–16. [https://doi.org/10.1016/0040-1951\(86\)90004-1](https://doi.org/10.1016/0040-1951(86)90004-1)
- Ho, T. T., Anh, T. T., Phuong, N. T., Dung, P. T., Anh, T. V., Izokh, A. E., et al. (2008). Permo-Triassic intermediate-felsic magmatism of the Truong son belt, eastern margin of Indochina. *Comptes Rendus Geosciences*, *340*(2-3), 112–126. <https://doi.org/10.1016/j.crte.2007.12.002>
- Holloway, N. (1982). North Palawan Block, Philippines; its relation to Asian mainland and role in evolution of South China Sea. *AAPG Bulletin*, *66*(9), 1355–1383.
- Hsu, S.-K., Yeh, Y.-c., Doo, W.-B., & Tsai, C.-H. (2004). New bathymetry and magnetic lineations identifications in the northernmost South China Sea and their tectonic implications. *Marine Geophysical Researches*, *25*(1–2), 29–44. <https://doi.org/10.1007/s11001-005-0731-7>
- Hu, D., Zhou, D., Wu, X., & He, M. (2008). Origin of high magnetic anomaly belt in northeastern South China Sea as indicated by geophysical inversion. *Journal of Tropical Oceanography*, *27*(1), 32–37.
- Huang, C., Zhou, D., Sun, Z., Chen, C., & Hao, H. (2005). Deep crustal structure of Baiyun Sag, northern South China Sea revealed from deep seismic reflection profile. *Chinese Science Bulletin*, *50*(11), 1131–1138. <https://doi.org/10.1360/04wd0207>
- Huang, C. C. (1963). Basic features of the tectonic structure of China (preliminary conclusion). *International Geology Review*, *1*, 73–88.
- Hutchison, C. S. (1989). *Geological evolution of South-east Asia*. Oxford: Clarendon Press.
- Hutchison, C. S. (1996). The 'Rajang accretionary prism' and 'Lupar Line' problem of Borneo. *Geological Society, London, Special Publications*, *106*(1), 247–261. <https://doi.org/10.1144/GSL.SP.1996.106.01.16>
- Hutchison, C. S. (2004). Marginal basin evolution: The southern South China Sea. *Marine and Petroleum Geology*, *21*(9), 1129–1148. <https://doi.org/10.1016/j.marpetgeo.2004.07.002>
- Isozaki, Y., Amiscaray, E. A., & Rillon, A. P. (1988). Permian, Triassic and Jurassic bedded radiolarian cherts in North Palawan Block, Philippines: Evidence of Late Mesozoic subduction-accretion. *IGCP Project*, *224*(3), 99–115.
- Jahn, B. M., Chen, P. Y., & Yen, T. P. (1976). Rb-Sr ages of granitic rocks in southeastern China and their tectonic significances. *Geological Society of America Bulletin*, *87*(5), 763–776. [https://doi.org/10.1130/0016-7606\(1976\)87<763:RAOGR>2.0.CO;2](https://doi.org/10.1130/0016-7606(1976)87<763:RAOGR>2.0.CO;2)
- Jahn, B. M., Martineau, F., Peucat, J. J., & Cornichet, J. (1986). Geochronology of the Tananao schist complex, Taiwan, and its regional tectonic significance. *Tectonophysics*, *125*(1–3), 103–124. [https://doi.org/10.1016/0040-1951\(86\)90009-0](https://doi.org/10.1016/0040-1951(86)90009-0)
- Jin, Q., & Li, T. (2000). Regional geologic tectonics of the Nansha Sea area. *Marine Science Bulletin/Haiyang Tongbao*, *2*(2). <https://doi.org/10.1029/2017JB014861>
- Jin, X. L. (1989). The geosciences research report in South China Sea (in Chinese). *Donghai Marine Science*, *7*, 30–42.
- John, B. M. (1990). Formation and tectonic evolution of SE China and Taiwan: Isotopic and geochemical constraints. *Tectonophysics*, *183*(1–4), 145–160. [https://doi.org/10.1016/0040-1951\(90\)90413-3](https://doi.org/10.1016/0040-1951(90)90413-3)
- Kido, Y., Suyehiro, K., & Kinoshita, H. (2001). Rifting to Spreading Process along the Northern Continental Margin of the South China Sea. *Marine Geophysical Research*, *22*, 1–15.
- Kogan, L., Fisseha, S., Bendick, R., Reilinger, R., McClusky, S., King, R., & Solomon, T. (2012). Lithospheric strength and strain localization in continental extension from observations of the East African Rift. *Journal of Geophysical Research*, *117*, B03402. <https://doi.org/10.1029/2011JB008516>
- Kudrass, H. R., Wiedicke, M., Cepek, P., Kreuzer, H., & Müller, P. (1986). Mesozoic and Cainozoic rocks dredged from the South China Sea (Reed Bank area) and Sulu Sea and their significance for plate-tectonic reconstructions. *Marine and Petroleum Geology*, *3*(1), 19–30. [https://doi.org/10.1016/0264-8172\(86\)90053-X](https://doi.org/10.1016/0264-8172(86)90053-X)
- Kushiro, I. (1974). Melting of hydrous upper mantle and possible generation of andesitic magma: An approach from synthetic systems. *Earth and Planetary Science Letters*, *22*(4), 294–299. [https://doi.org/10.1016/0012-821X\(74\)90138-1](https://doi.org/10.1016/0012-821X(74)90138-1)
- Kuszniir, N. J., & Park, R. G. (1987). The extensional strength of the continental lithosphere: Its dependence on geothermal gradient, and crustal composition and thickness. *Geological Society, London, Special Publications*, *28*(1), 35–52. <https://doi.org/10.1144/gsl.sp.1987.028.01.04>
- Lan, C. Y., Chung, S. L., Long, T. V., Lo, C. H., Lee, T. Y., Mertzman, S. A., & Shen, J. S. (2003). Geochemical and Sr-Nd isotopic constraints from the Kontum massif, central Vietnam on the crustal evolution of the Indochina block. *Precambrian Research*, *122*(1–4), 7–27. [https://doi.org/10.1016/S0301-9268\(02\)00205-X](https://doi.org/10.1016/S0301-9268(02)00205-X)
- Lang, Y. Q., Hu, D. Q., Liu, C., Zhang, B., & Lu, B. L. (2011). Mineralogy study of magnetic susceptibility of rocks along the coast of the northern South China Sea. *Chinese Journal of Geophysics*, *54*, 573–587.
- Lapierre, H., Jahn, B., Charvet, J., & Yu, Y. (1997). Mesozoic felsic arc magmatism and continental olivine tholeiites in Zhejiang Province and their relationship with the tectonic activity in southeastern China. *Tectonophysics*, *274*(4), 321–338. [https://doi.org/10.1016/S0040-1951\(97\)00009-7](https://doi.org/10.1016/S0040-1951(97)00009-7)
- Lei, J., Zhao, D., Steinberger, B., Wu, B., Shen, F., & Li, Z. (2009). New seismic constraints on the upper mantle structure of the Hainan plume. *Physics of the Earth and Planetary Interiors*, *173*(1–2), 33–50. <https://doi.org/10.1016/j.pepi.2008.10.013>
- Li, C., Li, J., Ding, W., Franke, D., Yao, Y., Shi, H., et al. (2015). Seismic stratigraphy of the central South China Sea basin and implications for neotectonics. *Journal of Geophysical Research: Solid Earth*, *120*, 1377–1399. <https://doi.org/10.1002/2014JB011686>
- Li, C. F., Shi, X., Zhou, Z., Li, J., Geng, J., & Chen, B. (2010). Depths to the magnetic layer bottom in the South China Sea area and their tectonic implications. *Geophysical Journal International*, *182*(3), 1229–1247. <https://doi.org/10.1111/j.1365-246X.2010.04702.x>
- Li, C. F., Xu, X., Lin, J., Sun, Z., Zhu, J., Yao, Y., & Zhang, G. (2014). Ages and magnetic structures of the South China Sea constrained by deep tow magnetic surveys and IODP Expedition 349. *Geochemistry, Geophysics, Geosystems*, *15*, 4958–4983. <https://doi.org/10.1002/2014GC005567>
- Li, C. F., Zhou, Z., Hao, H., Chen, H., Wang, J., Chen, B., & Wu, J. (2008). Late Mesozoic tectonic structure and evolution along the present-day northeastern South China Sea continental margin. *Journal of Asian Earth Sciences*, *31*(4–6), 546–561. <https://doi.org/10.1016/j.jseas.2007.09.004>
- Li, F., Sun, Z., & Zhang, J. (2018). Influence of mid-crustal rheology on the deformation behavior of continental crust in the continental subduction zone. *Journal of Geodynamics*, *117*, 88–99.
- Li, J. B., & Jin, X. L. (2008). *East Asia tectonic events and West Pacific Marginal Seas evolution* (pp. 443–451). Beijing: Ocean Press.
- Li, P. L., Liang, H. X., Dai, Y. D., & Lin, H. M. (1999). Origin and tectonic setting of the Yanshanian igneous rocks in the Pearl River mouth basin. *Guangdong Geology (in Chinese)*, *14*(1), 1–8.
- Li, P. L., Zhou, Z. C., & Chi, R. G. (1998). Basement structure and evolution of the Zhujiangkou basin. *Research Reports on Petroleum Geology of the Zhujiangkou Basin (East)*, *1*, 291–316.
- Li, S., Lin, C., Zhang, Q., Yang, S., & Wu, P. (1999). Episodic rifting of continental marginal basins and tectonic events since 10 Ma in the South China Sea. *Chinese Science Bulletin*, *44*(1), 10–23. <https://doi.org/10.1007/BF03182877>
- Li, X. H. (2000). Cretaceous magmatism and lithospheric extension in Southeast China. *Journal of Asian Earth Sciences*, *18*(3), 293–305. [https://doi.org/10.1016/S1367-9120\(99\)00060-7](https://doi.org/10.1016/S1367-9120(99)00060-7)

- Li, Z. X., & Li, X. (2007). Formation of the 1300-km-wide intracontinental orogen and postorogenic magmatic province in Mesozoic South China: A flat-slab subduction model. *Geology*, *35*(2), 179–182. <https://doi.org/10.1130/G23193A.1>
- Lu, B. L., Wang, P. J., Zhang, G. C., & Wang, W. Y. (2015). Characteristic of regional fractures in South China Sea and its basement tectonic framework. *Progress in Geophysics*, *30*(4), 1544–1553.
- Lundin, E. R., & Doré, A. G. (2011). Hyperextension, serpentinization, and weakening: A new paradigm for rifted margin compressional deformation. *Geology*, *39*(4), 347–350. <https://doi.org/10.1130/G31499.1>
- Maillet, P., Ruellan, E., Gérard, M., Person, A., Bellon, H., Cotten, J., et al. (1995). Tectonics, magmatism, and evolution of the New Hebrides Backarc troughs (Southwest Pacific). In B. Taylor (Ed.), *Backarc basins: Tectonics and magmatism* (pp. 177–235). Boston, MA: Springer. https://doi.org/10.1007/978-1-4615-1843-3_5
- Marquez, E. J., Aitchison, J. C., & Zamoras, L. R. (2006). Upper Permian to Middle Jurassic radiolarian assemblages of Busuanga and surrounding islands, Palawan, Philippines. *Swiss Journal of Geosciences*, *99*(1), 101–125.
- Marsh, B. D., & Carmichael, I. S. (1974). Benioff zone magmatism. *Journal of Geophysical Research*, *79*, 1196–1206. <https://doi.org/10.1029/JB079i008p01196>
- Maruyama, S., Isozaki, Y., Kimura, G., & Terabayashi, M. (1997). Paleogeographic maps of the Japanese Islands: Plate tectonic synthesis from 750 Ma to the present. *Island Arc*, *6*(1), 121–142. <https://doi.org/10.1111/j.1440-1738.1997.tb00043.x>
- Maus, S., Barckhausen, U., Berkenbosch, H., Bournas, N., Brozena, J., Childers, V., et al. (2009). EMAG2: A 2-arc min resolution Earth magnetic anomaly grid compiled from satellite, airborne, and marine magnetic measurements. *Geochemistry, Geophysics, Geosystems*, *10*, Q08005. <https://doi.org/10.1029/2009GC002471>
- Maus, S., Sazonova, T., Hemant, K., Fairhead, J., & Ravat, D. (2007). National geophysical data center candidate for the world digital magnetic anomaly map. *Geochemistry, Geophysics, Geosystems*, *8*, Q06017. <https://doi.org/10.1029/2007GC001643>
- Mayhew, M. A., Wasilewski, P. J., & Johnson, B. D. (1991). Crustal magnetization and temperature at depth beneath the yilgarn block, Western Australia inferred from magSAT data. *Earth and Planetary Science Letters*, *107*(3–4), 515–522. [https://doi.org/10.1016/0012-821X\(91\)90097-2](https://doi.org/10.1016/0012-821X(91)90097-2)
- McBirney, A. R. (1980). Mixing and unmixing of magmas. *Journal of Volcanology and Geothermal Research*, *7*(3–4), 357–371. [https://doi.org/10.1016/0377-0273\(80\)90038-4](https://doi.org/10.1016/0377-0273(80)90038-4)
- McCulloch, M. T., & Gamble, A. J. (1991). Geochemical and geodynamical constraints on subduction zone magmatism. *Earth and Planetary Science Letters*, *102*(2–3), 358–374.
- Morley, C. K. (2012). Late Cretaceous–Early Palaeogene tectonic development of SE Asia. *Earth-Science Reviews*, *115*(1–2), 37–75. <https://doi.org/10.1016/j.earscirev.2012.08.002>
- Nguyen, T. T. B., Satir, M., Siebel, W., & Chen, F. (2004). Granitoids in the Dalat zone, southern Vietnam: Age constraints on magmatism and regional geological implications. *International Journal of Earth Sciences*, *93*(3), 329–340.
- Nguyen, T. T. B., Satir, M., Siebel, W., Vennemann, T., & Long, T. V. (2004). Geochemical and isotopic constraints on the petrogenesis of granitoids from the Dalat zone, southern Vietnam. *Journal of Asian Earth Sciences*, *23*(4), 467–482.
- Nissen, S. S., Hayes, D. E., Bochu, Y., Weijun, Z., Yongqin, C., & Xiaopin, N. (1995). Gravity, heat flow, and seismic constraints on the processes of crustal extension: Northern margin of the South China Sea. *Journal of Geophysical Research*, *100*(B11), 22,447–22,483.
- Niu, Y. L. (2005). Generation and evolution of basaltic magmas: Some basic concepts and new views on the origin of Mesozoic–Cenozoic basaltic volcanism in eastern China. *Geological Journal of China Universities*, *11*, 9–46.
- Noda, A. (2016). Forearc basins: Types, geometries, and relationships to subduction zone dynamics. *Geological Society of America Bulletin*, *128*(5–6), 879–895. <https://doi.org/10.1130/B31345.1>
- Phan, C. T. (1992). Geology of Cambodia, Laos, and Vietnam: Explanatory Note to the Geological Map of Cambodia, Laos and Vietnam at 1:1,000,000 Scale, Geological Survey of Vietnam.
- Qiu, X. L., Zhao, M. H., Wei, A. O., Chuan-Chuan, L., Hao, T. Y., You, Q. Y., et al. (2011). OBS survey and crustal structure of the SW Sub-Basin and Nansha Block, South China Sea. *Chinese Journal of Geophysics*, *54*(6), 1009–1021. <https://doi.org/10.1002/cjg2.1680>
- Replumaz, A., & Tapponnier, P. (2003). Reconstruction of the deformed collision zone between India and Asia by backward motion of lithospheric blocks. *Journal of Geophysical Research*, *108*(B6), 2285. <https://doi.org/10.1029/2001JB000661>
- Ru, K., & Pigott, J. D. (1986). Episodic rifting and subsidence in the South China Sea. *AAPG Bulletin*, *70*(9), 1136–1155.
- Sales, A. O., Jacobsen, E. C., Morado, A. A., Benavidez, J. J., Navarro, F. A., & Lim, A. E. (1997). The petroleum potential of deep-water northwest Palawan Block GSEC 66. *Journal of Asian Earth Sciences*, *15*(2), 217–240.
- Schlüter, H., Hinz, K., & Block, M. (1996a). Tectono-stratigraphic terranes and detachment faulting of the South China Sea and Sulu Sea. *Marine Geology*, *130*(1–2), 39–78. [https://doi.org/10.1016/0025-3227\(95\)00137-9](https://doi.org/10.1016/0025-3227(95)00137-9)
- Sewell, R., & Campbell, S. (1997). Geochemistry of coeval Mesozoic plutonic and volcanic suites in Hong Kong. *Journal of the Geological Society*, *154*(6), 1053–1066. <https://doi.org/10.1144/gsjgs.154.6.1053>
- Shao, L., You, H., Hao, H., Wu, G., Qiao, P., & Lei, Y. (2007). Petrology and sedimentary environments of Mesozoic strata in the northeastern South China Sea. *Geological Review (in Chinese)*, *53*(2), 164–170.
- Shi, X., Burov, E., Leroy, S., Qiu, X., & Xia, B. (2005). Intrusion and its implication for subsidence: a case from the Baiyun Sag, on the northern margin of the South China Sea. *Tectonophysics*, *407*(1–2), 117–134.
- Soeparjadi, R. A., Valachi, L. Z., & Sosromihardjo, S. (1985). Oil and gas developments in Far East in 1984. *American Association of Petroleum Geologists Bulletin*, *69*(10), 1780–1855.
- Spector, A., & Grant, F. (1970). Statistical models for interpreting aeromagnetic data. *Geophysics*, *35*(2), 293–302. <https://doi.org/10.1190/1.1440092>
- Stern, R., & Smoot, N. C. (1998). A bathymetric overview of the Mariana forearc. *Island Arc*, *7*(3), 525–540.
- Stern, R. J., & Bloomer, S. H. (1992). Subduction zone infancy: Examples from the Eocene Izu-Bonin-Mariana and Jurassic California arcs. *GSA Bulletin*, *104*(12), 1621–1636. [https://doi.org/10.1130/0016-7606\(1992\)104<1621:SZIEFT>2.3.CO;2](https://doi.org/10.1130/0016-7606(1992)104<1621:SZIEFT>2.3.CO;2)
- Stern, R. J., Fouch, M. J., & Klempner, S. L. (2003). An overview of the Izu-Bonin-Mariana subduction factory, in Eiler, J., ed., *Inside the Subduction Factory*. *American Geophysical Union Geophysical Monograph*, *138*, 175–222. <https://doi.org/10.1029/138GM10>
- Sun, S., Li, J., Chen, H., Peng, H., Hsu, K. J., & Shelton, J. W. (1989). Mesozoic and Cenozoic sedimentary history of South China. *AAPG Bulletin*, *73*(10), 1247–1269.
- Sun, Z., Zhong, Z., Keep, M., Zhou, D., Cai, D., Li, X., et al. (2009). 3D analogue modeling of the South China Sea: A discussion on breakup pattern. *Journal of Asian Earth Sciences*, *34*(4), 544–556. <https://doi.org/10.1016/j.jseas.2008.09.002>
- Tapponnier, P., Lacassin, R., Leloup, P. H., Schärer, U., Zhong, D., Wu, H., et al. (1990). The Ailao Shan/Red River metamorphic belt: Tertiary left-lateral shear between Indochina and South China. *Nature*, *343*(6257), 431–437. <https://doi.org/10.1038/343431a0>
- Tapponnier, P., Peltzer, G., & Armijo, R. (1986). On the mechanics of the collision between India and Asia. In M. P. Coward & A. C. Ries (Eds.), *Collision tectonics, Spec. Publ.* (Vol. 19, pp. 115–157). London: Geol. Soc.

- Tapponnier, P., Peltzer, G., Le Dain, A. Y., Armijo, R., & Cobbold, P. (1982). Propagating extrusion tectonics in Asia: New insights from simple experiments with plasticine. *Geology*, *10*(12), 611–616. [https://doi.org/10.1130/0091-7613\(1982\)10<611:PETIAN>2.0.CO;2](https://doi.org/10.1130/0091-7613(1982)10<611:PETIAN>2.0.CO;2)
- Tatsumi, Y. (1982). Origin of high-magnesian andesites in the Setouchi volcanic belt, southwest Japan, II. Melting phase relations at high pressures. *Earth and Planetary Science Letters*, *60*(2), 305–317. [https://doi.org/10.1016/0012-821X\(82\)90009-7](https://doi.org/10.1016/0012-821X(82)90009-7)
- Taylor, B., & Hayes, D. E. (1980). The tectonic evolution of the South China Basin. *Geophysical Monograph Series*, *23*, 89–104.
- Taylor, B., & Hayes, D. E. (1983). Origin and history of the South China Sea basin. In D. E. Hayes (Ed.), *The tectonic and geologic evolution of Southeast Asian Seas and Islands: Part 2, Geophysical Monograph Series* (Vol. 27, pp. 23–56, 56). Washington, DC: American Geophysical Union.
- Thuy, N. T. B., Satir, M., Siebel, W., Vennemann, T., & Long, T. V. (2004). Geochemical and isotopic constraints on the petrogenesis of granitoids from the Dalat zone, southern Vietnam. *Journal of Asian Earth Sciences*, *23*(4), 467–482. <https://doi.org/10.1016/j.jseas.2003.06.001>
- Thybo, H., & Artemieva, I. M. (2013). Moho and magmatic underplating in continental lithosphere. *Tectonophysics*, *609*, 605–619.
- Tumanda, F. (1991). Radiolarian biostratigraphy in central Busuanga Island, Palawan, Philippines. *Journal of Geological Society of Philippines*, *46*, 49–104.
- Ubangoh, R. U., Pacca, I. G., Nyobe, J. L., Hell, J., & Ateba, B. (2005). Petrographic characteristics of Cameroon Line volcanic rocks. *Journal of Volcanology and Geothermal Research*, *142*(3–4), 225–241. <https://doi.org/10.1016/j.jvolgeores.2004.11.006>
- Vakhrameyev, V. A. (1983). Classification and correlation of continental deposits based on paleobotanic data. *International Geology Review*, *25*(1), 1–8.
- Wan, K., Xia, S., Cao, J., Sun, J., & Xu, H. (2017). Deep seismic structure of the northeastern South China Sea: Origin of a high-velocity layer in the lower crust. *Tectonophysics*, *700*, 2831–2858.
- Wang, D. Z., & Zhou, X. M. (2002). *Crustal evolution and petrogenesis of Late Mesozoic granitic volcanic-intrusive complexes in southeastern China* (pp. 1–295). Beijing: Science Press. (in Chinese with English Abstract)
- Wang, P. (2012). Tracing the life history of a marginal sea—On “The South China Sea Deep” Research Program. *Chinese Science Bulletin*, *57*(24), 3093–3114. <https://doi.org/10.1007/s11434-012-5087-1>
- Wei, X., Ruan, A., Zhao, M., Qiu, X., & Li, J. (2011). A wide-angle obs profile across the Dongsha Uplift and Chaoshan Depression in the Mid-Northern South China Sea. *Chinese Journal of Geophysics*, *54*(6), 3325–3335.
- Wu, F. Y., Lin, J. Q., Wilde, S. A., Zhang, X. O., & Yang, J. H. (2005). Nature and significance of the Early Cretaceous giant igneous event in eastern China. *Earth and Planetary Science Letters*, *233*(1–2), 103–119. <https://doi.org/10.1016/j.epsl.2005.02.019>
- Wu, G. X., Wang, R. J., Hao, H. J., & Shao, L. (2007). Microfossil evidence for development of marine Mesozoic in the north of South China Sea. *Marine Geology & Quaternary Geology*, *27*(1), 79–85.
- Wu, J. (1994). Evaluation and models of Cenozoic sedimentation in the South China Sea. *Tectonophysics*, *235*(1–2), 77–98. [https://doi.org/10.1016/0040-1951\(94\)90018-3](https://doi.org/10.1016/0040-1951(94)90018-3)
- Wu, J. M., & Yang, M. Z. (1994). Age analysis of seismic sequences in the southwestern South China Sea. *Geological Research of South China Sea*, *6*, 16–29. (in Chinese)
- Wu, Z. C., Gao, J. Y., Li, J. B., Zhang, T., Shen, Z. Y., & Yang, C. G. (2011). Characteristics of magnetic anomalies in the northern South China Sea and their implications for pre-Cenozoic tectonics. *Chinese Journal of Geophysics*, *54*(6), 113–118.
- Xia, K. Y., & Huang, C. L. (2004). Distribution and hydrocarbon potential of Upper Triassic to Cretaceous strata in South China Sea and adjacent areas. *China Offshore Oil and Gas (in Chinese)*, *16*, 73–83.
- Xie, X., Müller, R. D., Li, S., Gong, Z., & Steinberger, B. (2006). Origin of anomalous subsidence along the Northern South China Sea margin and its relationship to dynamic topography. *Marine and Petroleum Geology*, *23*(7), 745–765. <https://doi.org/10.1016/j.marpetgeo.2006.03.004>
- Xie, Y., Tong, C., Fan, C., Peng, S., Hao, Z., & Tong, H. (2015). Characteristics and evolution of fault system in Qiongdongnan Basin. *Geotectonica Et Metallogenia (in Chinese)*, *5*, 795–807.
- Xiu, C., Zhang, D. J., Di, S. K., Liu, X. Y., & Bi, D. J. (2016). Zircon U-Pb age of Granitic rocks from the basement beneath the Shi Island, XISHA Islands and its geological significance. *Marine Geology & Quaternary Geology*, *36*(3), 115–126. (in Chinese)
- Xu, G. Q., Wu, S. H., Zhang, L., Li, X. G., Yi, H., Lei, L., & Xu, X. (2013). Stratigraphic division and depositional processes for the Mesozoic basin in northern South China Sea. *Marine Geophysical Research*, *34*(3–4), 175–194. <https://doi.org/10.1007/s11001-013-9201-9>
- Xu, Y., Wei, J., Qiu, H., Zhang, H., & Huang, X. (2012). Opening and evolution of the South China Sea constrained by studies on volcanic rocks: Preliminary results and a research design. *Chinese Science Bulletin*, *57*(24), 3150–3164. <https://doi.org/10.1007/s11434-011-4921-1>
- Yan, P., Deng, H., Liu, H. L., Zhang, Z. R., & Jiang, Y. K. (2006). The temporal and spatial distribution of volcanism in the South China Sea region. *Journal of Asian Earth Sciences*, *27*(5), 647–659. <https://doi.org/10.1016/j.jseas.2005.06.005>
- Yan, P., & Liu, H. (2004). Tectonic-stratigraphic division and blind fold structures in Nansha Waters, South China Sea. *Journal of Asian Earth Sciences*, *24*(3), 337–348. <https://doi.org/10.1016/j.jseas.2003.12.005>
- Yan, P., Zhou, D., & Liu, Z. (2001). A crustal structure profile across the northern continental margin of the South China Sea. *Tectonophysics*, *338*(1), 1–21.
- Yan, Q., Shi, X., & Castillo, P. R. (2014). The late Mesozoic–Cenozoic tectonic evolution of the South China Sea: A petrologic perspective. *Journal of Asian Earth Sciences*, *85*, 178–201. <https://doi.org/10.1016/j.jseas.2014.02.005>
- Yan, Q., Shi, X., Liu, J., Wang, K., & Bu, W. (2010). Petrology and geochemistry of Mesozoic granitic rocks from the Nansha micro-block, the South China Sea: Constraints on the basement nature. *Journal of Asian Earth Sciences*, *37*(2), 130–139. <https://doi.org/10.1016/j.jseas.2009.08.001>
- Yan, Q., Shi, X., Wang, K., Qingdao, & An, X. (2008). LA-ICPMS zircon U-Pb dating of granitic rocks from the Nansha micro-block, South China Sea, and its geological significance. *Acta Geologica Sinica (in Chinese)*, *82*(8), 1057–1067.
- Yao, B. (1996). Tectonic evolution of the South China Sea in Cenozoic. *Marine Geology & Quaternary Geology (in Chinese)*, *16*(2), 1–13.
- Yao, B., Zeng, W., Chen, Y., Zhang, X., Hayes, D., Diebold, J., et al. (1994). The crustal structure in the eastern part of the northern margin of the South China Sea. *Acta Geophys Sin (in Chinese)*, *37*(1), 27–35.
- Yumul, G. P. (2007). Westward younging disposition of Philippine ophiolites and its implication for arc evolution. *Island Arc*, *16*(2), 306–317. <https://doi.org/10.1111/j.1440-1738.2007.00573.x>
- Zamorras, L. R., and A. Matsuoka (2001). Malampaya Sound Group: a Jurassic–Early Cretaceous accretionary complex in Busuanga Island, North Palawan block (Philippines)(0016–7630).
- Zamorras, L. R., & Matsuoka, A. (2004). Accretion and postaccretion tectonics of the Calamian Islands, North Palawan block, Philippines. *Island Arc*, *13*(4), 506–519. <https://doi.org/10.1111/j.1440-1738.2004.00443.x>
- Zhang, J., Sun, Z., & Zhang, S. (2014). Analysis of Mesozoic tectonic deformation in the Chaoshan Depression of Pearl River Mouth Basin. *Journal of Tropical Oceanography (in Chinese)*, *33*(5), 41–49.

- Zhang, L., Zhang, G. X., & Wang, L. L. (2014). *The distribution of Mesozoic in the northern South China Sea margin and its hydrocarbon resources potential* (pp. 54–64). Beijing: Geological Publishing House. (in Chinese)
- Zhang, Q., Wu, S. G., Lv, F. L., Dong, D. D., Yan, Q. S., & Yang, Z. (2014). The seismic characteristics and the distribution of the igneous rocks in the northernwest slope of the South China Sea. *Geotectonica et Metallogenia (in Chinese)*, 38(4), 919–938.
- Zhao, M. S., Liu, H. L., & Chao-Hua, W. U. (2012). Mesozoic stratigraphic and structural features and collisional orogeny between the northern and southern continental margins of South China Sea. *Progress in Geophysics (in Chinese)*, 27(4), 1454–1464.
- Zhao, Y., Ren, J., Pang, X., Yang, L., & Zheng, J. (2018). Structural style, formation of low angle normal fault and its controls on the evolution of Baiyun rift, northern margin of the South China Sea. *Marine and Petroleum Geology*, 89, 687–700. <https://doi.org/10.1016/j.marpetgeo.2017.11.001>
- Zhou, D. (2002). Mesozoic strata and sedimentary environment in SW Taiwan Basin of NE South China Sea and Peikang high of western Taiwan. *Journal of Tropical Oceanography (in Chinese)*, 21(2), 50–57.
- Zhou, D., Chen, H. Z., & Sun, Z. (2004). *Mesozoic lithofacies and paleo-geography of South China Sea and adjacent areas and related tectonic and resource issues* (pp. 65–76). Beijing: Marine Press.
- Zhou, D., Liu, H., & Chen, H. (2005). Mesozoic-Cenozoic magmatism in southern South China Sea and its surrounding areas and its implications to tectonics. *Geotectonica Et Metallogenia (in Chinese)*, 29(3), 339–345.
- Zhou, D., Sun, Z., Chen, H., Xu, H., Wang, W., Pang, X., et al. (2008). Mesozoic paleogeography and tectonic evolution of South China Sea and adjacent areas in the context of Tethyan and Paleo-Pacific interconnections. *Island Arc*, 17(2), 186–207. <https://doi.org/10.1111/j.1440-1738.2008.00611.x>
- Zhou, D., Wang, W., Wang, J., Pang, X., Cai, D., & Sun, Z. (2006). Mesozoic subduction-accretion zone in northeastern South China Sea inferred from geophysical interpretations. *Science in China Series D*, 49(5), 471–482. <https://doi.org/10.1007/s11430-006-0471-9>
- Zhou, M., Liu, H., & Wu, C. (2013). Mesozoic stratigraphic and structural features and collisional orogeny between the northern and southern continental margins of the South China Sea. *Progress in Geophysics*, 27(4), 1454–1464.
- Zhou, X., & Li, W. (2000). Origin of late Mesozoic igneous rocks in southeastern China: Implications for lithosphere subduction and underplating of mafic magmas. *Tectonophysics*, 326(3–4), 269–287. [https://doi.org/10.1016/S0040-1951\(00\)00120-7](https://doi.org/10.1016/S0040-1951(00)00120-7)
- Zhou, X. M., Sun, T., Shen, W. Z., Shu, L. S., & N. Y. L. (2006). Petrogenesis of Mesozoic granitoids and volcanic rocks in South China: A response to tectonic evolution. *Episodes*, 29(1), 26–33.